AMERICAN SOCIETY of
GENE & CELL
THERAPY

RBP EIF2S2 Promotes Tumorigenesis and Progression by Regulating MYC-Mediated Inhibition via FHIT-Related Enhancers

Jiwei Zhang,[1,8] Shengli Li,[5,8] Ling Zhang,[6,8] Juan Xu,[2,3,4] Mingxu Song,[7] Tingting Shao,[4] Zhaohui Huang,[7] and Yongsheng Li[2,3,4]

[1]The MOE Key Laboratory for Standardization of Chinese Medicines, Institute of Chinese Materia Medica, Shanghai University of Traditional Chinese Medicine, Shanghai 201203, China; [2]Key Laboratory of Tropical Translational Medicine of Ministry of Education, Hainan Medical University, Haikou 571199, China; [3]College of Biomedical Information and Engineering, Hainan Medical University, Haikou 571199, China; [4]College of Bioinformatics Science and Technology, Harbin Medical University, Harbin, Heilongjiang 150081, China; [5]Department of Biochemistry and Molecular Biology, The University of Texas Health Science Center at Houston McGovern Medical School, Houston, TX 77030, USA; [6]College of Life Science, Zhejiang Chinese Medical University, Hangzhou 310009, China; [7]Wuxi Cancer Institute, Affiliated Hospital of Jiangnan University, 200 Huihe Road, Wuxi Shi, Jiangsu Province 214123, China

RNA-binding proteins (RBPs) play fundamental roles in cancer; however, we still lack knowledge about to what extent RBPs are dysregulated, as well as about perturbed signaling pathways in cancer. In this study, we integrated analysis of multidimensional data across >10,000 cancer patients and >1,000 cell lines. We identified a top candidate RBP: eukaryotic translation initiation factor 2 subunit beta (EIF2S2). EIF2S2 is highly expressed in tumors and is associated with malignant features as well as patient prognosis. Functional assays performed in cancer cells revealed that EIF2S2 promotes cancer cell proliferation, migration, and invasion *in vitro* as well as tumor growth and metastasis *in vivo*. Mechanistic investigations further demonstrated that EIF2S2 promotes tumorigenesis and progression by directly binding to a long non-coding RNA, LINC01600, which physically interacts with the MYC protein and increases its stability. Interestingly, we revealed that the EIF2S2-LINC01600-MYC axis can activate the Wnt/β-catenin pathway by inhibiting the activity of FHIT-related enhancers and FHIT expression. Finally, EIF2S2 knockdown combined with oxaliplatin treatment could be a potential combination therapy in cancer. Our integrated analysis provided detailed knowledge of the function of the EIF2S2-LINC01600-MYC axis, which will facilitate the development of rational combination therapies for cancer.

INTRODUCTION

Gastrointestinal (GI) cancers are among the most common invasive, lethal tumors.[1,2] Despite tremendous advancements in therapeutic strategies, the overall survival rate has not yet been improved.[3] The initiation and maintenance of tumors are centered on the concept of cancer hallmarks via genetic and epigenetic mechanisms.[4] Although a number of oncogenes and tumor suppressor genes have been identified in GI cancers,[5,6] we still lack knowledge about the landscape of transcriptome perturbations and the regulators that contribute to cancer development.

Compelling evidence has shown that RNA-binding proteins (RBPs) play important roles in regulating gene expression and have a pivotal role in many human diseases, especially cancers.[7,8] Currently, an increasing number of RBPs have been curated,[9,10] and some have been demonstrated to drive tumorigenicity and progression. Dang et al.[11] demonstrated that NELFE functions as an oncogenic protein and contributes to transcriptome imbalance in hepatocellular carcinoma (HCC) via MYC signaling. In addition, the RBP quaking (QKI) was shown to function as a principal regulator in the differentiation of colonic epithelium, the deregulation of which is involved in the onset and progression of colon cancer.[12] Epithelial splicing regulatory protein 1 (ESRP1) has been reported to act as a pro-oncogenic RBP in colorectal cancer (CRC) by modulating tumor growth.[13] These observations suggest that RBPs are key mediators of oncogenic transcriptomic changes.

Moreover, the biggest problems in anticancer drug development are acquired multidrug resistance and relapse.[14] Oxaliplatin (1,2-diaminocyclohexane-oxalate platinum) is a third-generation platinum compound with anti-cancer activity in CRC,[15] gastric cancer (GC), and many other tumors. However, cancer patients treated with these drugs often develop drug resistance. Studies have reported possible mechanisms of oxaliplatin resistance, including increased drug detoxification,[16] changes in apoptosis-regulating genes,[17] and
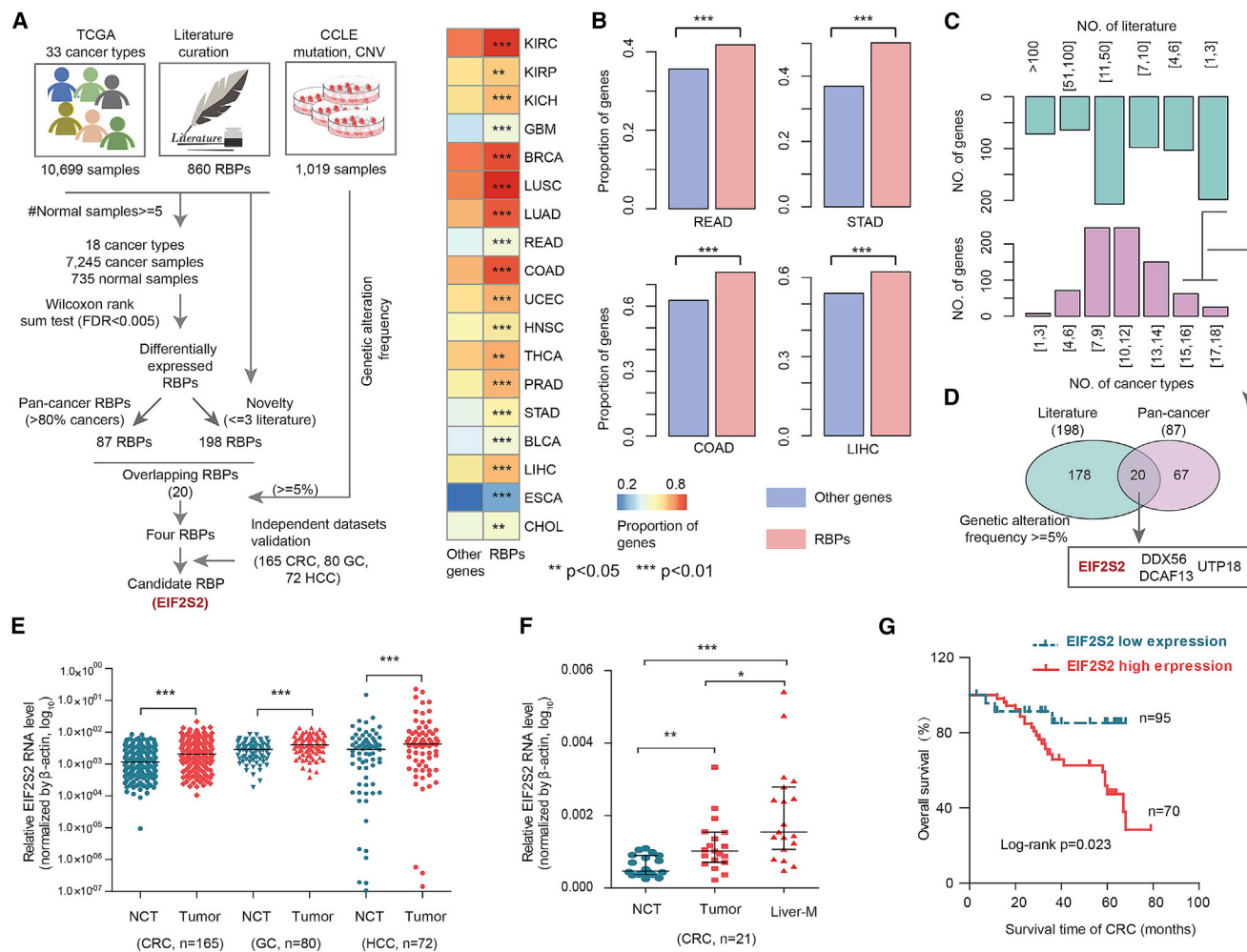
Figure 1. Integrative Analyses of Multidimensional Omics Data Revealed Candidate RBPs in Human Cancers

(A) Flowchart for identifying critical RBPs in cancer. (B) Heatmap showing the proportion of differentially expressed RBPs and other genes. The bar plots on the right show the results for four types of gastrointestinal cancer. Fisher's exact test. (C) The top bar plot shows the number of publications reporting RBPs, and the bottom bar plot shows the number of cancer types in which the RBPs were dysregulated. (D) Venn diagram shows the overlap of pan-cancer RBPs and less frequently reported RBPs. (E) Relative RNA levels of EIF2S2 in CRC, GC, and HCC patients. Red indicates tumor patients; cyan indicates normal controls. Wilcoxon signed-rank test. (F) Relative RNA level of EIF2S2 in normal controls and patients with CRC and liver metastasis. Wilcoxon signed-rank test. (G) Kaplan-Meier survival analysis of CRC and HCC patients stratified by the EIF2S2 gene expression level. p = 0.023, log-rank test. *p < 0.05, **p < 0.01, ***p < 0.001.

enhancement of the DNA damage repair capacity.[18] These studies revealed the complicity of oxaliplatin resistance, but the detailed underlying mechanisms are still poorly understood. One popular solution to the enduring challenge of drug resistance is rational combinatorial targeted therapy.[19] Thus, it is critical to identify regulators that can result in impressive therapeutic effects of oxaliplatin in GI cancers.

In this study, we integrated multiple omics data from >10,000 tumor samples and >1,000 cell lines and found that RBPs are more likely than other proteins to be perturbed in cancer. Specifically, we identified a critical RBP regulator, eukaryotic translation initiation factor 2 subunit beta (EIF2S2), in GI cancer. EIF2F2 is upregulated in CRC, GC, and HCC, and its upregulation is significantly associated with

the malignant features and poor outcomes of patients. Systematic investigation showed that the EIF2S2-LINC01600-MYC axis can bind to the enhancer region of FHIT, further inhibiting the regulatory effect of FHIT on the Wnt signaling pathway. Finally, our results suggested that EIF2S2 silencing combined with oxaliplatin is a potential therapeutic strategy for GI cancers.

RESULTS

Global Analyses of RBPs Identify Aberrant EIF2S2 Expression in GI Cancers

To characterize the transcriptional alterations in RBPs across cancer types, we first assembled 860 RBPs from the literature.[9] Next, we identified differentially expressed RBPs in 18 cancer types (Figure 1A).

Table 1. Relationships between EIF2S2 Expression and Clinical Pathological Features of Patients with CRC

Parameter	No. of Patients	EIF2S2 (Low)	EIF2S2 (High)	p Value
Sex				
Male	92	44	48	0.288
Female	73	33	40	
Age (years)				
<60	69	28	41	0.176
≥60	96	54	42	
Distant Metastasis				
Absent	62	23	39	0.062
Present	103	30	73	
Tumor Size (cm)				
≤5	80	36	28	0.214
>5	85	28	29	
Location				
Colon	102	34	58	0.056
Rectum	63	18	45	
Depth of Tumor				
T1+T2	57	18	39	0.036
T3+T4	98	32	66	
Vascular Invasion				
Absent	72	42	30	0.218
Present	93	32	61	
Nervous Invasion				
Absent	70	32	68	0.469
Present	95	10	11	
Lymphatic Metastasis				
Absent	92	57	35	0.018
Present	73	33	40	
Differentiation Grade				
I–II	65	32	33	0.025
III–IV	100	28	72	

Interestingly, we observed that transcriptional perturbations in RBPs were common events in almost all cancer types (Figure 1B, p < 0.05 for all cancer types). For instance, more than 60% of RBPs were differentially expressed in colon adenocarcinoma (COAD; p < 0.01) and HCC (p < 0.01). These results reveal the widespread transcriptional perturbations in RBPs across cancer types, particularly GI cancer.

To further screen key RBPs in human cancers, we first identified 87 RBPs that were differentially expressed in more than 80% of cancer types (Figure 1C; Table S1). By querying the PubMed database, we concluded that most of these RBPs were involved in tumorigenesis and progression (Figure 1C). To identify novel cancer-related RBPs, we focused on 20 RBPs that were reported in fewer than three publications (Figure 1D; Table S1). In addition, we integrated the genomic

alteration data from 1,019 cell lines and found that four RBPs (EIF2S2, DDX56, DCAF13, and UTP18) showed genomic alterations in more than 5% of cell lines. DDX56 was identified as an oncogene in CRC by promoting the splicing of WEE1.[20] DCAF13 was associated with the survival of HCC and breast cancer.[21,22] UTP18 is a component of the small subunit processome and is frequently gained and overexpressed in cancer.[23] Of these RBPs, EIF2S2 was more significantly aberrantly expressed than the other three RBPs and was selected for further study.

EIF2S2 catalyzes the exchange of GDP (guanosine 5′-diphosphate) for GTP (guanosine 5′-triphosphate) during the translation initiation steps of protein synthesis, and little is known about its role in tumorigenesis. Moreover, we collected independent gene expression data across CRC, GC, and liver cancer patients. We found that EIF2S2 also exhibited significantly higher expression in cancer (Figure S1A). We also evaluated the expression of EIF2S2 in 317 paired tumor tissues and corresponding noncancerous tissues (NCTs), including 165 CRCs, 80 GCs, and 72 HCCs (Table 1). We found that EIF2S2 was more highly expressed in tissues from these the three types of cancers than in the corresponding NCTs (Figure 1E, all p values <0.001). Moreover, higher EIF2S2 expression was observed in liver metastasis samples than in primary CRC tumors (Figure 1F). To investigate the determinants of higher expression of EIF2S2, we first analyzed the copy number of EIF2S2 across patients in TCGA. We found that EIF2S2 was amplified across the majority of cancer types, particular in CRC (Figure S1B). Next, we also performed quantitative polymerase chain reaction (qPCR) to investigate copy number variations in EIF2S2 in 70 CRCs, 30 GCs, and 30 HCCs. Higher copy number amplification of EIF2S2 was observed in these cancer samples than in their corresponding NCTs (Figures S2A–S2C). Finally, we explored the effects of EIF2S2 on prognosis in GI cancer patients and revealed that high expression of EIF2S2 is associated with poor survival of CRC (Figure 1G, p = 0.023) and HCC patients (Figure S2D, p = 9.1E−6 and 0.012). Taken together, these results suggested that EIF2S2 plays oncogenic roles in GI cancers.

EIF2S2 Promotes Tumor Growth and Progression in GI Cancers

To further analyze the effects of EIF2S2 on GI cancers, we knocked down or overexpressed EIF2S2 in CRC, GC, and HCC cell lines (Figures S3A–S3C) and then performed colony and cell proliferation assays. We found that EIF2S2 is highly expressed in HCT-116 cells and lowly expressed in LoVo cells. Thus, we performed functional experiments in LoVo and HCT-116 cell lines. We demonstrated that silencing EIF2S2 expression significantly inhibited CRC, GC, and HCC cell colony formation (Figures 2A–2C; Figure S3D) and proliferation (Figure 2D). In contrast, EIF2S2 overexpression significantly promoted the colony formation and proliferation abilities of cancer cells (Figures 2A–2D; Figure S3D). We next explored the roles of EIF2S2 in cell invasion and metastasis. The results of the Matrigel invasion assay showed that EIF2S2 knockdown significantly decreased migration and invasion (Figures 2F–2H; Figures S3E and S3F), whereas ectopic EIF2S2 expression significantly enhanced the migration and invasion of GI cancer cells (Figures 2F–2H; Figures S3E and
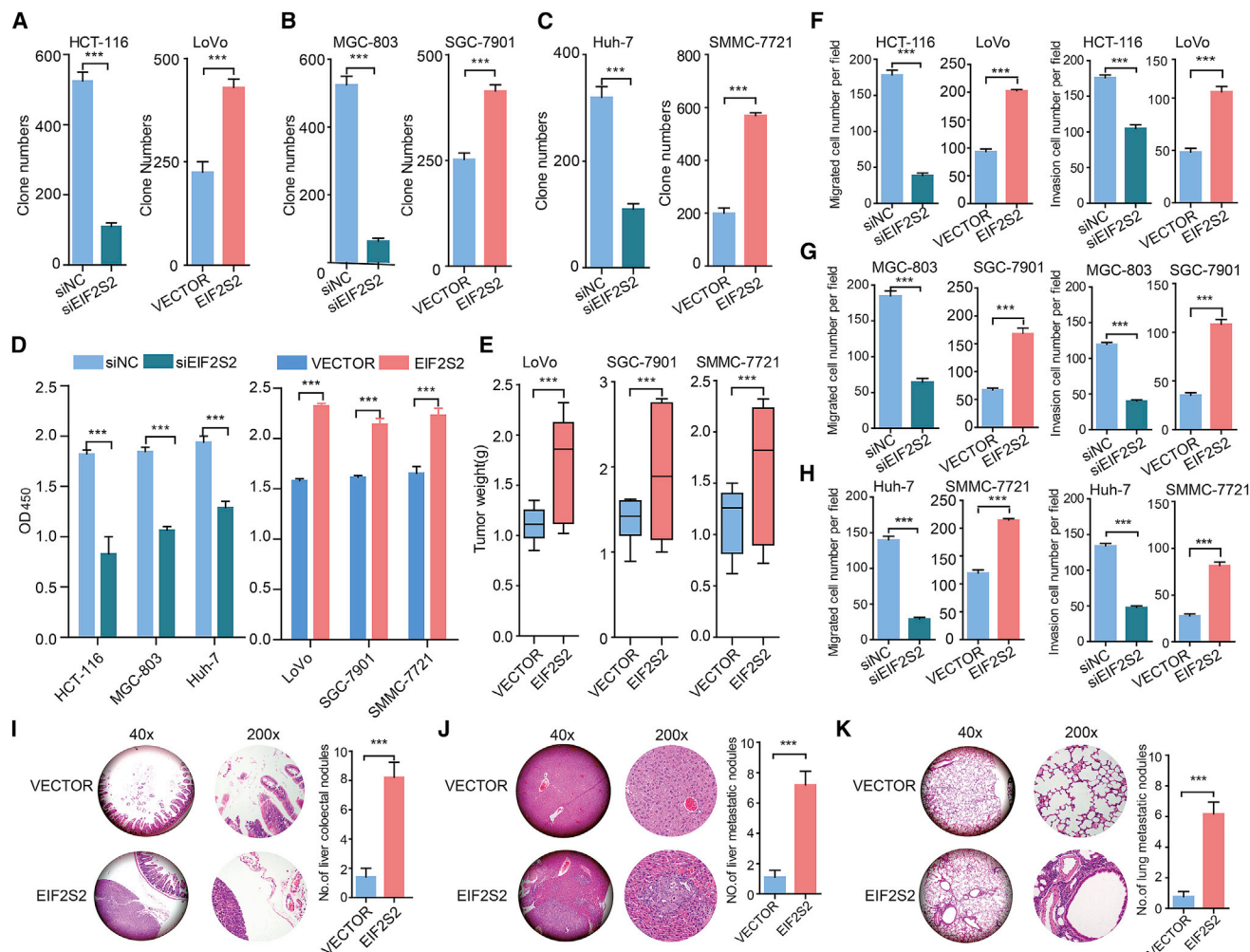
Figure 2. EIF2S2 Increases GI Cancer Cell Proliferation, Invasion, and Metastasis _In Vitro_ and _In Vivo_

(A–C) Colony formation assays of the effects of siEIF2S2 or pWPXL-EIF2S2 treatment in CRC, GC, and HCC cell lines. (A) HCT-116 and LoVo; (B) MGC-803 and SGC-7901; and (C) Huh-7 and SNU-449. (D) Cell Counting Kit-8 (CCK-8) assays showing the growth of CRC, GC, and HCC cells treated with siEIF2S2 (left) or pWPXL-EIF2S2 (right). (E) Tumor weights were measured in the pWPXL-EIF2S2 and negative control groups in the xenograft mouse models. (F–H) Transwell migration and invasion assays in CRC (F), GC (G), and HCC (H) cell lines treated with siEIF2S2 or pWPXL-EIF2S2. (I–K) The number of metastatic foci in the intestine (I), liver (J), and lungs (K) of nude mice at 6 weeks after injection with stable pWPXL-EIF2S2 LoVo cells. The values are presented as means ± standard error of the mean (SEM), n = 3. ***p < 0.001, Wilcoxon signed-rank test.

S3F). Taken together, these results demonstrated that EIF2S2 significantly promotes the _in vitro_ migration and invasion of GI cancer cells.

To confirm the effects of EIF2S2 on the tumorigenicity of GI cancer cells, EIF2S2-overexpressing cells and control cells, derived from the LoVo, SGC-7901, and SNU-449 cell lines, were subcutaneously injected into nude mice. After 8 weeks, the volume and weight of tumors were dramatically increased in the EIF2S2 group compared with the control groups (Figure 2E; Figures S3G–S3I), suggesting that overexpression of EIF2S2 markedly promoted the tumorigenic ability of GI cancers. Next, EIF2S2-overexpressing cells and control cells derived from SNU-449 cells were transplanted into the intestine, liver, and tail vein of nude mice. After 6 weeks, the mice were sacri-

ficed and the nodules were examined. We observed that 90% (9/10) of mice implanted EIF2S2-overexpressing cells had colorectal metastatic nodules, whereas only 10% of mice in the control group did (Figure 2I; Figure S3J; p = 0.0007). Moreover, 70% (7/10) of mice implanted with EIF2S2-overexpressing cells had distal lung metastases, whereas 20% of mice in the control group did (Figure 2J; Figure S3J; p = 0.0011). Regarding lung metastasis, 60% (6/10) of mice in the EIF2S2 group and no mice in the vector group developed metastatic nodules (Figure 2K; Figure S3J; p = 0.0032). These findings demonstrate that EIF2S2 significantly promotes GI cancer metastasis.

EIF2S2 Preferentially Promotes Wnt Signaling

To further investigate the oncogenic roles of EIF2S2, we performed gene set enrichment analysis (GSEA)[24] based on the genome-wide

expression profiles of CRC from The Cancer Genome Atlas (TCGA) project. We first calculated the Spearman correlation between the expression of EIF2S2 and that of all other genes. Next, genes were ranked based on the correlation and were then subjected to GSEA analysis. In this study, we focused on the signaling pathways in Reactome.[25] We found that genes positively coexpressed with EIF2S2 were significantly enriched in the "signaling by WNT" pathway in both COAD and rectal adenocarcinoma (READ) datasets (Figures S4A–S4C, p < 0.001), suggesting that Wnt signaling is a key downstream pathway regulated by EIF2S2.

Next, we investigated the expression levels of several representative genes in the WNT signaling pathway in EIF2S2-depleted or EIFS2S-overexpressing CRC cells. Most of the genes in the WNT pathway showed expression perturbations in EIF2S2-overexpressing or EIF2S2 knockdown tumor cells (Figure S4D). Particularly, we found that the protein levels of ROCK2 and c-Myc were increased or decreased in EIF2S2-overexpressing or EIF2S2-depleted CRC cells, respectively (Figure S4E). Moreover, the activity of the luciferase reporter-containing response element of the core WNT signaling pathway component β-catenin was augmented in EIF2S2-overexpressing CRC cells (Figure S4F, p < 0.001). In contrast, the reporter activity was diminished after EIF2S2 knockdown (Figure S4F, p < 0.001). These results suggest that EIF2S2 might exert its tumor-promoting functions by modulating the WNT signaling pathway.

EIF2S2 Coordinately Regulates with MYC through Binding to LINC01600

Although EIF2S2 has been previously identified as an RBP,[9] its targets are largely unknown. Genetic studies have proven that a significant number of non-coding RNAs (ncRNAs) are associated with GI cancers,[26] and the expressions of long ncRNAs (lncRNAs) are tightly regulated by RBPs.[27] Thus, we hypothesized that EIF2S2 may bind to specific ncRNAs to exert its carcinogenic functions in cancer cells. We measured the expression of ncRNAs using RNA sequencing (RNA-seq) and found that one lncRNA (LINC01600) showed significant downregulation after knockdown of EIF2S2 (Figure S5A). LINC01600 has been reported to be upregulated in lung cancer and associated with poor prognosis.[28] However, little is known about its roles in human cancers. The primary LINC01600 transcript of 2,434 bp was identified by 5′ and 3′ RACE and northern blot assays in LoVo and HCT-116 cells (Figures S5B and S5C). Next, we measured the expression of LINC01600 and found that it was variable in CRC cell lines (Figure S5D), with a nuclear distribution of approximately 54% (Figure S5E). Importantly, there was a strong positive correlation between the expression of LINC01600 and EIF2S2 in CRC tissues (correlation coefficient [r] = 0.84, p < 0.0001; Figure S5F). In addition, overexpression of EIF2S2 significantly increased LINC01600 expression, while knockdown of EIF2S2 significantly reduced the expression of LINC01600 (Figure S5G). Furthermore, we observed that LINC01600 was significantly upregulated in CRC tissues compared with NCTs (n = 165, Figure S5H). In the 21 CRCs with liver metastasis, we found higher LINC01600 expression in metastatic samples than in primary tumors (Figure S5I, all

p values < 0.05). Importantly, patients with higher LINC01600 levels exhibited poorer overall survival than did those with lower levels (Figure S5J, p = 0.018). In particular, significantly shorter survival times were observed in patients with high expression of both EIF2S2 and LINC01600 (Figure S5K, p = 0.0004). These results suggest that LINC01600 plays critical roles associated with EIF2S2 in GI cancers.

To further explore the molecular mechanism by which EIF2S2 regulates LINC01600 in CRC cells, we performed biotin-labeled RNA pull-down accompanied by mass spectrometry to identify LINC01600-interacting proteins. The results of three independent experiments consistently showed two specific proteins of approximately 60 and 45 kDa in the LINC01600 pull-down samples (Figure 3A). We obtained seven potential interacting proteins based on a confidence score cutoff of >50 in mass spectrometry (Figure 3A). Notably, we found that c-MYC, a key signaling molecule in the WNT pathway,[29] was confirmed as a specific binding protein of LINC01600. In addition, EIF2S2 was associated with LINC01600 (Figure 3A). The results of a western blotting assay using the retrieved protein samples in the RNA pull-down assay further confirmed the binding of EIF2S2 and c-MYC to LINC01600 (Figure 3B, top panels). These interactions were further confirmed through RNA immunoprecipitation (RIP) assays (Figure 3B, bottom panels). These results suggest that LINC01600 can bind to EIF2S2 and c-MYC in CRC. Furthermore, we found that the 5′ fragment (nucleotides 1–379) of LINC01600 was responsible for the interaction with EIF2S2 (Figure 3C), and the 3′ fragment (nucleotides 1,831–2,000) with c-MYC (Figure 3C).

To explore whether EIF2S2 and c-MYC bind each other through a link with LINC01600, we performed coimmunoprecipitation experiments with EIF2S2 and c-MYC. We found that EIF2S2 can interact with c-MYC (Figure 3D, top panels). However, LINC01600 knockdown significantly blocked the interaction between EIF2S2 and c-MYC (Figure 3D, bottom panels). These results indicate that LINC01600 acts as a scaffold in the interaction between EIF2S2 and c-MYC. Next, we performed RIP assays to determine the interaction region of EIF2S2 and c-MYC. We found that deletion of the domain presented in eiF2B (eiF2B_5, amino acids 199–308), eIF5 of EIF2S2, significantly abolished the association of EIF2S2 with LINC01600 (Figure 3E). In addition, deletion of some helix-loop-helix (HLH) domains (amino acids 370–426) in c-MYC exhibited similar effects (Figure 3F), indicating that LINC01600 binds to EIF2S2 and c-MYC through these regions, respectively. These results indicate that both EIF2S2 and c-MYC specifically bind with LINC01600, and that LINC01600 plays a scaffolding role to link c-MYC to EIF2S2 in CRC cells.

EIF2S2 Enhances the Stability of the MYC Protein by Reducing the Degradation of LINC01600

We next characterized the molecular consequences of the associations among EIF2S2, c-MYC, and LINC01600. Interestingly, the activity of the luciferase reporter containing the c-MYC response element was diminished in EIF2S2-silenced cells, and it was augmented after LINC01600 overexpression (Figure 4A).
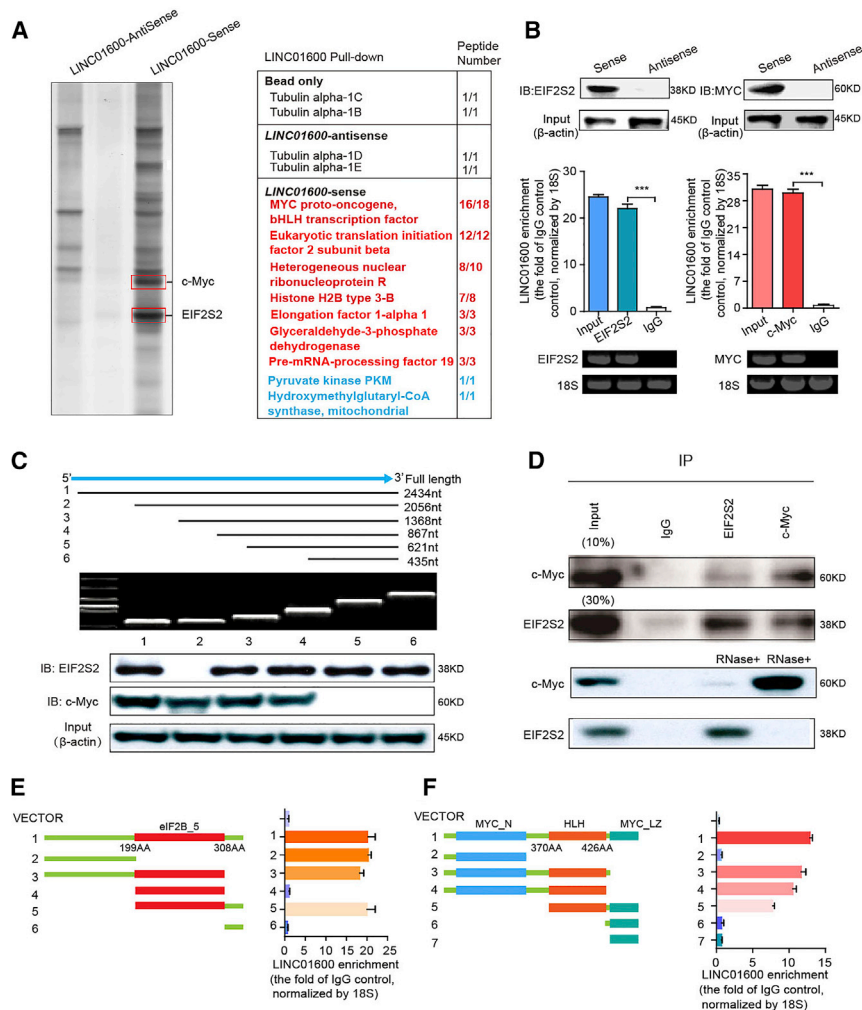
Figure 3. EIF2S2 Interacts with LINC01600 and MYC
(A) RNA pull-down experiments with biotinylated-sense LINC01600 or biotinylated-antisense LINC01600. Specific bands identified by MS are shown in the right panel. (B) Immunoblotting for the specific association of EIF2S2, and MYC with biotinylated-LINC01600 from three independent streptavidin RNA pull-down assays (top panel). Real-time PCR was used to detect LINC01600 enrichment, using immunoglobulin G (IgG) antibody as a control (middle panel). 18S rRNA was also used as a control (bottom panel). ***p < 0.001, Wilcoxon signed-rank test. (C) Immunoblotting of EIF2S2 and MYC in samples from pulldown assays with full-length biotinylated LINC01600 or truncated biotinylated LINC01600 RNA segments, with GAPDH as a negative control. (D) Immunoprecipitation to detect the association between EIF2S2 and endogenous MYC (top panel) in HCT-116 cells with LINC01600 overexpression or knockdown. (E and F) RNA immunoprecipitation analysis for LINC01600 enrichment in cells transiently transfected with plasmids containing the indicated full-length or truncated constructs. Deletion mapping for domains of EIF2S2 (E) and MYC (F) that bind to LINC01600 is shown.

steady-state level of LINC01600, whereas depletion of EIF2S2 resulted in decreases in the half-life and RNA level of LINC01600 (Figure 4B). These results suggest that EIF2S2 specifically regulates the stability of LINC01600 in CRC cells. However, LINC01600 had no effect on the protein levels of EIF2S2 but showed an obvious effect on the c-MYC protein levels (Figure 4C). Moreover, after treatment with the protein-synthesis inhibitor cycloheximide (CHX), LINC01600 knockdown decreased the half-life of c-MYC protein, whereas ectopic LINC01600 expression increased the half-life of the c-MYC protein in CRC cells (Figure 4D). These results indicate that LINC01600 might inhibit the proteasome-dependent degradation of c-MYC in CRC cells. Furthermore, the ubiquitination levels of c-Myc were significantly decreased in LINC01600-OE cells, whereas the ubiquitination levels of c-Myc were increased in LINC01600-knockdown cells (Figure 4E). LINC01600 overexpression rescued the effects of EIF2S2 knockdown on the expression of c-MYC target genes, whereas silencing of LINC01600 expression significantly decreased the expression levels of the genes induced by ectopic expression of EIF2S2 (Figure 4F), suggesting that EIF2S2 might regulate the expression of c-MYC downstream genes through modulation of LINC01600. Moreover, LINC01600 knockdown notably abolished the promotive effects of EIF2S2 on cell proliferation, migration, and invasion, whereas LINC01600 overexpression abrogated the inhibitory effects of EIF2S2 knockdown on cell proliferation, migration, and invasion (Figures 4G–4I; Figure S7). Taken together, these findings demonstrate that EIF2S2 acts as an oncogenic driver by activating c-MYC through LINC01600 in CRC cells.

Particularly, EIF2S2 and LINC01600 double knockdown significantly decreased activity of the c-MYC reporter in CRC cells significantly (Figure 4A). Alternatively, overexpression of EIF2S2 promoted the activity of the c-MYC reporter, while ectopic LINC01600 expression in EIF2S2-overexpressing CRC cells further promoted the activity of the c-MYC reporter (Figure 4A). To investigate the function of LINC01600 in CRC cell lines, cell lines with stable overexpression (pWPXL-LINC01600) and knockdown (shLINC01600) were established (Figure S6A). We found that LINC01600 overexpression significantly enhanced CRC cell proliferation, colony formation, migration, and invasion (Figures S6B–S6E, all p values <0.001). In contrast, LINC01600 knockdown significantly inhibited cell proliferation, colony formation ability, cell migration, and invasion (Figures S6B–S6E, all p values < 0.001). These results suggest that LINC01600 plays a carcinogenic role.

Actinomycin D, which effectively inhibits *de novo* synthesis of RNA, was used to explore the effects of EIF2S2 on the stability of LINC01600. Overexpression of EIF2S2 increased the half-life and
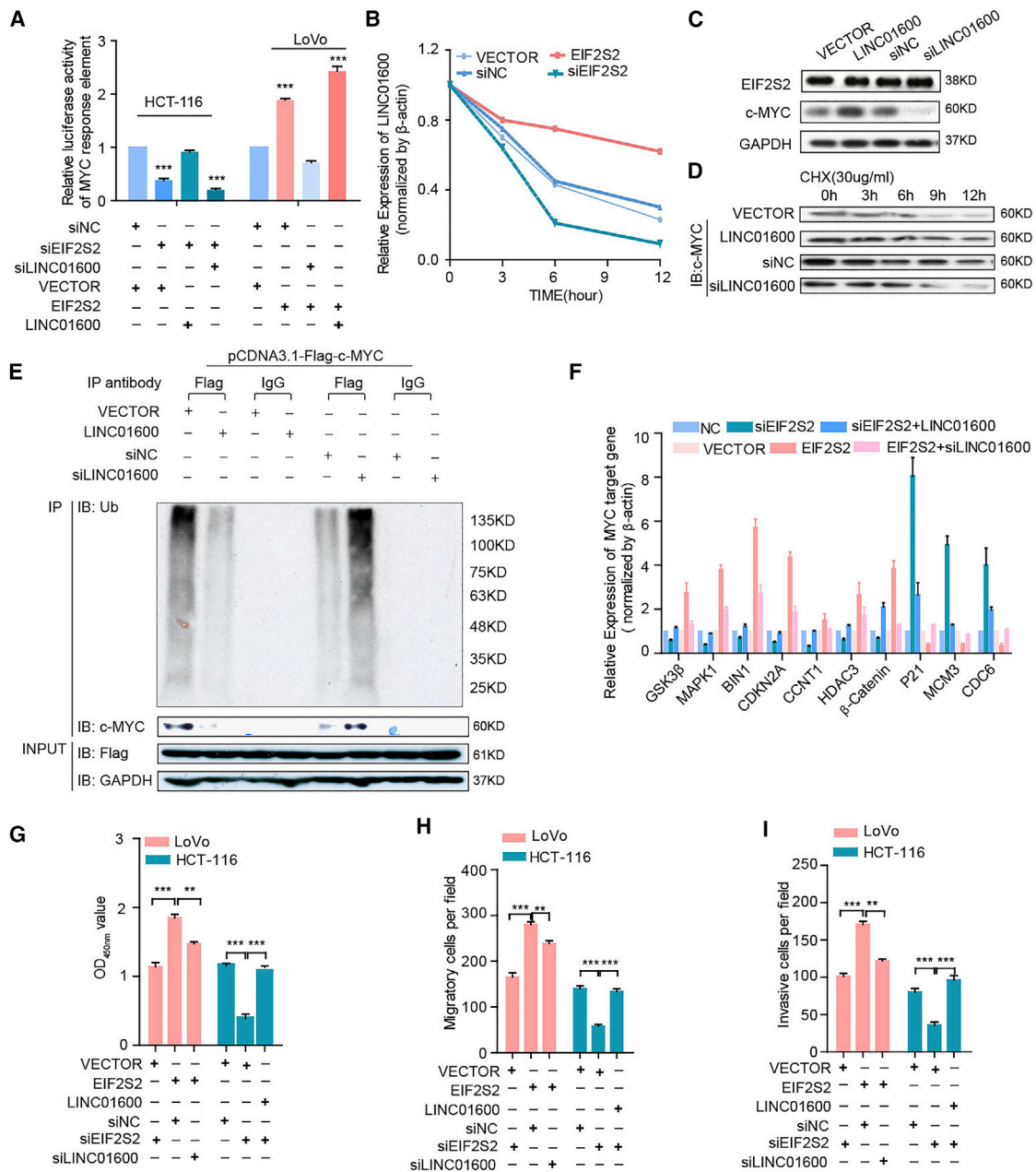
Figure 4. EIF2S2 Plays Oncogenic Roles by Blocking the Proteasomal Degradation of MYC in a LINC01600-Dependent Manner

(A) Luciferase assays in CRC cells infected with lentivirus expressing EIF2S2 or transfected with EIF2S2 after LINC01600 knockdown or overexpression. Wilcoxon signed-rank test. (B) Densitometric analysis of LINC01600 RNA levels in cells with EIF2S2 knockdown or overexpression. The relative fold changes are expressed compared to the level at 0 h. (C) Immunoblotting to measure the EIF2S2 and MYC protein levels in cancer cells with ectopic expression of LINC01600 or treated with siLINC01600. (D) Immunoblotting to measure the MYC levels in cells with ectopic expression of LINC01600 or treated with siLINC01600 and cycloheximide (CHX, 30 μg/mL) for different durations. (E) Cells with LINC01600 knockdown or overexpression were transfected with pCMV-Flag-c-Myc plasmids for 48 h. Cell lysates were immunoprecipitated (IP) with either control IgG or anti-Flag antibody and immunoblotted with ubiquitin-specific antibody. Flag-tagged c-Myc and GAPDH served as the loading controls. (F) The relative mRNA levels of MYC downstream genes in HCT-116 and LoVo cells infected with lentivirus expressing EIF2S2/LINC01600 or transfected with EIF2S2/LINC01600 small interfering RNAs (siRNAs). (G–I) Proliferation (G), migration (H), and invasion assays (I) in HCT-116 and LoVo cells infected with lentivirus expressing EIF2S2/LINC01600 or transfected with EIF2S2/LINC01600 siRNAs. **$p < 0.01$, ***$p < 0.001$, Wilcoxon signed-rank test.
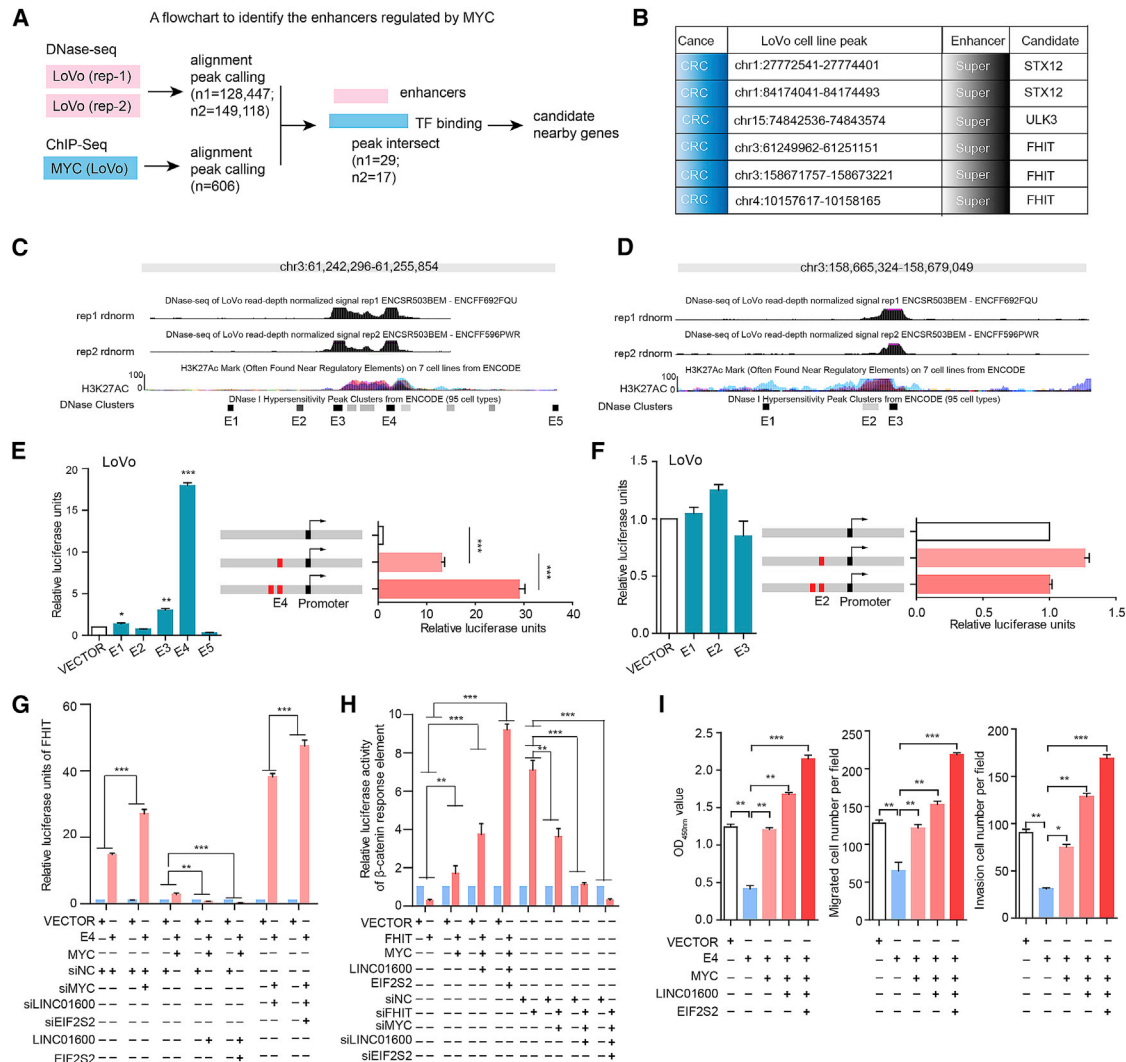
Figure 5. The Activity of FHIT Is Predominantly Driven by the E4 Constituent Enhancer

(A) The workflow for identifying MYC-regulated enhancers and target genes. (B) Candidate genomic regions harboring enhancers and adjacent target genes in the LoVo cell line. (C and D) Genomic overview of the DNase and H3K27ac signals in two representative enhancers of FHIT (C, super-enhancer I; D, super-enhancer II). E1E5 were enhancers. (E and F) Luciferase reporter assays were used to measure the enhancer activity of constituent enhancers in LoVo cells. The pCDH plasmid without the enhancer region (empty) was used as a negative control (E, super-enhancer I; F, super-enhancer II). (G) Relative expression of FHIT in LoVo cells with different treatments. (H) Luciferase reporter assays for β-catenin activity in LoVo cells with different treatments. (I) The effect of the FHIT E4 enhancer on proliferation (left panel), migration (middle panel), and invasion (right panel) in cells was dependent on the EIF2S2-LINC01600-MYC axis. *p < 0.05, **p < 0.01, ***p < 0.001, Wilcoxon signed-rank test.

The EIF2S2-LINC01600-MYC Axis Regulates Enhancers in Cancer

To further investigate the functional consequence of the EIF2S2-LINC01600-MYC complex, we next integrated the DNase-seq and chromatin immunoprecipitation sequencing (ChIP-seq) data to identify its downstream targets. We identified 606 genomic regions that were bound by c-MYC. By determining the intersection of these genomic regions, we identified 29 and 17 noncoding regions for further analyses (Figure 5A). Specifically, we focused on six candidate regions that were defined as super-enhancers in this study (Figure 5B). Two distinct focal regions located ∼1 and ∼97,420 kb far away from

the FHIT gene in CRC cells were further investigated (Figures 5C and 5D). Interestingly, the tumor suppressor FHIT was demonstrated to play an unexpected role in the regulation of β-catenin-mediated gene transcription.[30] To determine the functions of FHIT-related enhancers, we integrated DNase clusters in 95 cell types and identified five nearby constituent enhancers (E1–E5) and three distant constituent enhancers (E1′–E3′). These candidate enhancers overlapped with H3K27ac signals (Figures 5C and 5D). Next, luciferase reporter assays were performed to investigate the functions of these enhancers. We found that the E4 enhancer showed the strongest activity in LoVo cells (Figures 5E and 5F). However, there was no detectable enhancer

activity in HEK293 cells, confirming that this super-enhancer was specific to CRC. Furthermore, duplication of the E4 enhancer in the luciferase reporter construct resulted in a >2-fold increase in luciferase expression relative to that of the construct with a single copy of E4 (Figure 5E). These results indicate that an increase in the copy number of the enhancer region may upregulate the expression of target genes.

Interestingly, we found that the expression of FHIT was significantly increased or decreased in E4-overexpressing or E4-depleted CRC cells, respectively (Figure S8A). In addition, we found that FHIT functions as a tumor suppressor in CRC and that dysregulated expression of FHIT is significantly involved in cell proliferation, migration, and invasion (Figures S8B–S8D). Moreover, we found that knockdown of the E4 enhancer significantly promoted cancer cell proliferation, migration, and invasion (Figures S8E and S8F). In contrast, overexpression of E4 produced the opposite effects (Figures S8E and S8F). These results suggest that the enhancer E4 plays critical roles in cancer development and progression by directly regulating the tumor suppressor FHIT. Furthermore, c-MYC knockdown markedly promoted the regulatory effect of the enhancer E4 on FHIT transcription, which was further repressed by overexpression of EIF2S2 and LINC01600 (Figure 5G). Alternatively, E4 restoration significantly restored the expression levels of FHIT, which were decreased by c-MYC, and FHIT expression was further activated by knockdown of EIF2S2 and LINC01600 (Figure 5G). Next, we further investigated the effects of the EIF2S2-LINC01600-MYC axis on the Wnt signaling pathway. We found that FHIT significantly inhibited the activity of the Wnt pathway, which was regulated by the EIF2S2-LINC01600-MYC axis (Figure 5H). Moreover, restoration of c-MYC markedly blocked the inhibitory effects of E4 on cell proliferation, migration, and invasion, which were further restored by overexpression of EIF2S2 and LINC01600 (Figure 5I). Taken together, these findings demonstrate that EIF2S2, LINC01600, and MYC formed a complex to regulate the E4 enhancer region, which further inhibits the regulatory effect of FHIT on the Wnt signaling pathway in CRC cells.

EIF2S2 Is a Candidate Therapeutic Target for GI Cancers

Because EIF2S2 expression was found to be significantly associated with poor patient survival and increased tumor growth in GI cancers, it may be a good candidate therapeutic target. Thus, we next assessed the potential effect of EIF2S2 on sensitivity to oxaliplatin, the most commonly used drug for CRC treatment.[31] We first assessed EIF2S2 and c-MYC protein expression levels and LINC01600 RNA levels using immunohistochemistry (IHC) and qPCR, respectively, in 35 paired CRC tissues, and NCTs and the corresponding oxaliplatin-resistant tissue specimens. The expression levels of EIF2S2, c-MYC, and LINC01600 were significantly higher in oxaliplatin-resistant patients (Figures 6A and 6B, p < 0.001). In addition, there was strong positive correlation between the expression of EIF2S2 and LINC01600 in oxaliplatin-resistant tissue specimens (Figure 6C, r = 0.70, p < 0.001).

Next, we investigated the effects of EIF2S2 and LINC01600 on oxaliplatin sensitivity. We demonstrated that ectopic EIF2S2 expression significantly decreased the sensitivity of CRC cells to oxaliplatin compared with that of cells treated with the vector control (50% inhibitory concentration [IC_{50}], 19.5 versus 7.48 nM) (Figure 6D, left panel), whereas LINC01600 knockdown restored the sensitivity of these cells to oxaliplatin (Figure 6D, right panel). Notably, the IC_{50} of oxaliplatin in EIF2S2-silenced cells was dramatically decreased, by ~89% relative to that in control cells (Figure 6E, left panel), whereas overexpression of LINC01600 blocked siEIF2S2-induced chemo-sensitization to oxaliplatin (Figure 6E, right panel). These results suggest that EIF2S2 is a key factor accounting for oxaliplatin resistance in CRC. To further assess the effect of EIF2S2 on chemo-resistance to oxaliplatin *in vivo*, we established a xenograft tumor model in nude mice. We observed that EIF2S2 knockdown significantly reduced the tumor growth compared to that in the control group (Figure 6F). Furthermore, an *in situ* mouse intestinal perfusion model was used to evaluate the effect of EIF2S2 on oxaliplatin resistance. The results showed that the number of metastatic foci derived from EIF2S2 knockdown tumors was dramatically decreased in the intestinal and liver tissues (Figures 6G and 6H, all p values <0.001). These results suggest that EIF2S2 could be a potential therapeutic target in CRC.

DISCUSSION

Accumulating studies have revealed that RBPs regulate the expression of thousands of transcripts,[32] and some have been reported to be involved in various types of cancer.[33,34] Discovering the driver RBPs in cancer is critical for precision oncology. In the present study, we integrated multidimensional genomic and transcriptomic data from ~10,000 tumor patients and ~1,000 cancer cell lines in the TCGA and Cancer Cell Line Encyclopedia (CCLE) projects. Our integrative analyses revealed a top candidate RBP, EIF2S2, which plays oncogenic roles in GI cancers. Our work provides several lines of evidence to support the model indicating that the oncogenic EIF2S2-LINC01600-MYC axis blocks the inhibitory effect of FHIT on the WNT signaling pathway in cancer (Figure 6I). Specifically, we found that EIF2S2, LINC01600, and MYC are highly expressed in CRC (Figure S9A). These oncogenic molecules form a lncRNA-centered complex and further suppress the regulatory effect of FHIT on the WNT signaling. Specifically, we demonstrated that siEIF2S2 treatment combined with oxaliplatin treatment may be a potential therapeutic approach in CRC.

With the development of high-throughput sequencing, an increasing number of lncRNAs have been identified.[35] However, little is known about the functions of these lncRNAs.[36,37] lncRNAs are involved in various types of biological functions through diverse mechanisms, often including interactions with protein partners.[27,38] In the current study, we identified LINC01600 as a candidate target of EIF2S2 and demonstrated that this lncRNA plays an oncogenic role in GI cancers. Furthermore, we validated that LINC01600 interacts with the MYC protein. The oncogenic role of c-MYC has been thoroughly investigated in cancer development
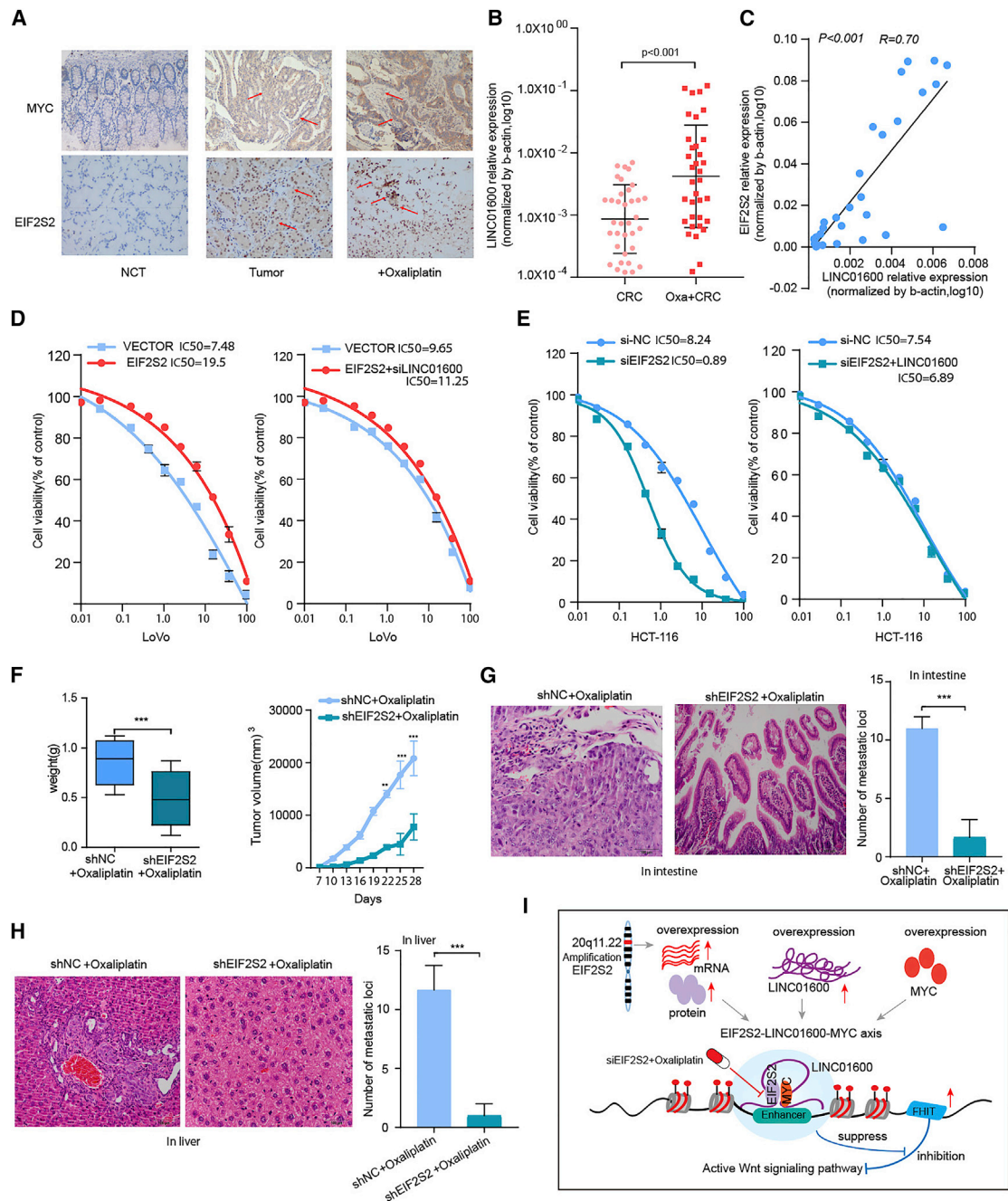
Figure 6. Combination Treatment with siEIF2S2 and Oxaliplatin in CRC

(A) IHC images indicating EIF2S2 and MYC expression levels in adjacent normal tissues, CRC tissues, and oxaliplatin-resistant intestinal cancer tissues (original magnification, ×200). (B) LINC01600 RNA expression levels in CRC tissues and oxaliplatin-resistant intestinal cancer tissues. (C) Scatterplot of gene expression correlations between EIF2S2 and LINC01600 in CRC oxaliplatin-resistant intestinal cancer tissues. (D) Distribution of IC_{50} values in cells transfected with EIF2S2 or the EIF2S2-siLINC01600 mixture, and exposed to oxaliplatin for 3 days. (E) The distribution of the IC_{50} values in cells transfected with siEIF2S2 or the siEIF2S2-pWPXLLINC01600 mixture and exposed to oxaliplatin for 3 days. (F) Tumor weights and volumes in nude mice bearing subcutaneous tumor xenografts from shNC (control) cells or shEIF2S2 cells injected *in situ* with oxaliplatin. (G) Number of metastatic loci in the intestines of mice treated with oxaliplatin and shEIF2S2+oxaliplatin. (H) Number of metastatic loci in the livers of mice treated with oxaliplatin and shEIF2S2+oxaliplatin. The values are expressed as the means ± SEM. *p < 0.05, **p < 0.01, ***p < 0.001, Wilcoxon signed-rank test. (I) Proposed model depicting the role of EIF2S2 as an oncogene in CRC.

and progression.[39,40] MYC can be activated by multiple mechanisms in cancer, and emerging evidence has uncovered the role of lncRNAs, such as CCAT1-L (CRC-associated transcript 1),[41] PCGM1 (prostate cancer gene expression marker 1),[42] GHET1 (gastric carcinoma highly expressed marker 1),[43] and EPIC1 (epigenetically induced lncRNA1),[44] in MYC activation. In this study, we reveal that LINC01600 can bind to the HLH domain of MYC and further stabilize the MYC protein. These results suggest that LINC01600 may function as a "guide" RNA to facilitate EIF2S2-MYC regulation on MYC targets, further activating the Wnt signaling pathway. Since MYC amplification is the cancer-driven event, we next explored whether there is an association between EIF2S2 overexpression and MYC amplification. We found that although there was higher expression in the MYC-amplified patients, the difference was not significant (p = 0.215). These results suggest that EIF2S2 overexpression was likely to be an independent cancer-driven event.

Encouraged by the recapitulation of MYC function, we mechanistically validated the hypothesis that the EIF2S2-LINC01600-MYC axis can regulate the function of FHIT-related enhancers. Similar to our findings, focal amplification of different enhancer regions downstream of MYC has been reported in other cancer types.[45,46] Interestingly, we found that FHIT is a tumor suppressor that is highly expressed in cancers (Figure S9B). FHIT can inhibit the activity of the Wnt signaling pathway. We demonstrated that the EIF2S2-LINC01600-MYC axis can suppress the inhibitory effect of FHIT on Wnt signaling, providing a potential explanation for the activation of Wnt signaling in cancer. Moreover, oxaliplatin is the first platinum drug with proven activity to treat CRC.[47] However, only subsets of patients respond to this treatment. It is important to identify a new therapeutic approach to overcome oxaliplatin resistance.[48] Because the dysregulation of RBPs can affect many pathways of cancer, RBPs might be good therapeutic targets.[49] There are several clinical trials for targeting RBPs as cancer therapy. Intravenous injection of antisense oligonucleotide (ASO) against eIF4E can suppress tumor growth without any side effect.[50] In addition, siHuR has shown dramatic anti-oncogenic activity in cancer.[51] In this study, we demonstrated that decreased EIF2SE expression appears to be a major contributor to chemosensitivity to oxaliplatin treatment, suggesting a rational combination of EIF2S2i and oxaliplatin. Moreover, we found that the expression of EIF2S2 is associated with poor prognosis of patients in various types of cancer (Figure S9C). These data suggest that EIF2S2 silencing has the potential to increase the effectiveness of oxaliplatin treatment. Clinical trials are needed to determine whether the combination of siEIF2S2 and oxaliplatin will benefit these patients. All of these results suggest that identification of RBPs can be developed as therapeutic drugs for cancer therapy.

In summary, our results provide a detailed knowledge base for the function of the EIF2S2-LINC01600-MYC axis in cancer. Our integrative analysis reveals a candidate driver RBP, and the mechanistic characterization of EIF2S2 helps to pave the way for the development of cancer therapies.

MATERIALS AND METHODS

Clinical Samples and Cell Lines
We collected 79 paired human CRC tissues and NCTs at the Affiliated Hospital of Jiangnan University, and 86 paired CRC tissues and NCTs at Fudan University Zhongshan Hospital. The patient information is shown in Table 1. In addition, a total of 80 pairs of human primary GC tissues and adjacent NCTs were collected between 2008 and 2012 at the Affiliated Hospital of Jiangnan University. The tissue samples were immediately snap frozen in liquid nitrogen and were histologically confirmed. Another 72 paired HCC samples and adjacent NT liver tissues from patients with HCC were obtained from the surgical specimen archives of Fudan University Zhongshan Hospital, Shanghai, China. All of these human materials were obtained with informed consent.

Cells were cultured following the instructions recommended by the American Type Culture Collection (ATCC). HEK293T cells were purchased from ATCC, and human GC cell lines (MGC-803 and SGC-7901) were purchased from Shanghai Meixuan. The CRC cell lines LoVo, Caco2, HT29, HCT8, HCT116, CCH-HE-2, DLD1, and SW480 were purchased from ATCC between 2008 and 2014. Huh-7 cells were obtained from the Japanese Collection of Research Bioresources (JCRB, Tokyo, Japan). The SNU-449 cell line was purchased from the Shanghai Cell Bank Type Culture Collection Committee (CBTCCC, Shanghai, China). All media (HyClone, USA) were supplemented with 10% fetal bovine serum (FBS) (Gibco, USA). SGC-7901, MKN45, and HEK293T cells were cultured in DMEM. This study was carried out with the permission of the Clinical Research Ethics Committees of the Affiliated Hospital of Jiangnan University and the Institutional Review Board of the Shanghai Medical College of Fudan University.

Gene Expression Analysis of Human RBPs across Cancer Types
We assembled 860 RBPs from a recent study.[9] Next, we obtained genome-wide gene expression data across 10,699 samples of 33 cancer types from the TCGA project.[52] Gene expression was measured as fragments per kilobase of transcript per million mapped reads (FPKM). First, we excluded the genes that were not expressed in more than 30% of the samples. Next, the gene expression values were log transformed. To identify the RBPs that are perturbed in cancer, we used the Wilcoxon rank-sum test to identify the RBPs differentially expressed in cancer. Here, only the 18 cancer types with more than five corresponding normal samples were considered. The p values were adjusted by the Benjamini-Hochberg procedure. RBPs with adjusted p values <0.005 were considered differentially expressed in cancer.

Identification of Critical RBPs in GI Cancer
To evaluate whether RBPs were more likely than other proteins to be perturbed in cancer, we first calculated the proportion of RBP-encoding genes that showed transcriptomic perturbations and the proportion of other genes perturbed in cancer. The differences between the two proportions were compared with Fisher's exact test. Next, to

identify the critical RBPs in cancer, we first identified RBPs that show transcriptional perturbations in more than 80% of cancer types. Moreover, we used the corresponding gene symbols and "cancer" as keywords to query the PubMed database for these RBPs. This process was performed with the R package RISmed (https://rdrr.io/cran/RISmed/). We focused on the RBPs reported in fewer than three publications and obtained 20 RBPs. Moreover, we obtained the genomic alterations in 1,019 cell lines from the CCLE project.[53] We calculated the genetic alteration frequency (including all types of somatic mutations and copy number variations) for each RBP across the cell lines. We found that four RBPs had a frequency of >5%. These RBPs were identified as critical RBPs in cancer.

GSEA

To identify the pathways potentially regulated by EIF2S2, we first calculated the expression correlation coefficient for each gene with EIF2S2. In this study, we analyzed the gene expression data from the COAD, READ, and LIHC projects in TCGA.[54] We next ranked all genes based on the correlation coefficient, and these genes were subjected to GSEA analysis (see details in Supplemental Materials and Methods).[24,55] The signaling pathways from Reactome were considered.[25]

Identification of the Candidate Enhancer Targets of MYC

We obtained the DNase-seq peak files in the LoVo cell line from the Encyclopedia of DNA Elements (ENCODE) project. In this study, two replicates were analyzed separately. In addition, we downloaded the MYC binding sites obtained from ChIP-seq data in the LoVo cell line. After mapping the reads to the human genome, we obtained 128,447 and 149,118 regulatory regions in LoVo cells. The peak coordinates were transformed to the hg38 version by liftover.[56] Next, we used BEDtools to obtain the overlapped genomic region from the DNase-seq and ChIP-seq data.[57] Finally, the genes nearest these peaks were taken as candidate target genes.

Supporting Materials and Methods

For details regarding the RNA pull-down assays and mass spectrometry analyses, RNA immunoprecipitation assay, DNA and RNA isolation, western blotting, Northern blot, 5′ and 3′ RACE assay, subcellular fractionation, cell proliferation and colony formation assays, invasion and migration assays, luciferase assay, *in vivo* assays, RNA interference and generation of lentivirus particles, immunoblotting analysis, IHC, *in vitro* cellular IC_{50} assays, and other related procedures, refer Supplemental Materials and Methods and Table S2. Mixed clone cells of EIF2S2 stable cell lines were used in our current study.

Statistical Analysis

All data are presented as mean ± standard deviation (SD) of at least three independent experiments. The Kaplan-Meier method was used to determine overall survival rates, and the p values were calculated with the log-rank test. A Wilcoxon rank sum test was used to identify the differentially expressed RBPs. All statistical analyses

were performed using R 3.5.1 program. A p value of <0.05 was considered to indicate statistical significance.

SUPPLEMENTAL INFORMATION

Supplemental Information can be found online at https://doi.org/10.1016/j.ymthe.2020.02.004.

REFERENCES

1. Peery, A.F., Crockett, S.D., Murphy, C.C., Lund, J.L., Dellon, E.S., Williams, J.L., Jensen, E.T., Shaheen, N.J., Barritt, A.S., Lieber, S.R., et al. (2019). Burden and cost of gastrointestinal, liver, and pancreatic diseases in the United States: update 2018. Gastroenterology 156, 254–272.e11.

2. Moehler, M., Delic, M., Goepfert, K., Aust, D., Grabsch, H.I., Halama, N., Heinrich, B., Julie, C., Lordick, F., Lutz, M.P., et al. (2016). Immunotherapy in gastrointestinal cancer: recent results, current studies and future perspectives. Eur. J. Cancer 59, 160–170.

3. Kemi, N., Eskuri, M., Ikäläinen, J., Karttunen, T.J., and Kauppila, J.H. (2019). Tumor budding and prognosis in gastric adenocarcinoma. Am. J. Surg. Pathol. 43, 229–234.

4. Hanahan, D., and Weinberg, R.A. (2011). Hallmarks of cancer: the next generation. Cell 144, 646–674.

5. Forbes, S.A., Beare, D., Boutselakis, H., Bamford, S., Bindal, N., Tate, J., Cole, C.G., Ward, S., Dawson, E., Ponting, L., et al. (2017). COSMIC: somatic cancer genetics at high-resolution. Nucleic Acids Res. 45 (D1), D777–D783.

6. Forbes, S.A., Beare, D., Gunasekaran, P., Leung, K., Bindal, N., Boutselakis, H., Ding, M., Bamford, S., Cole, C., Ward, S., et al. (2015). COSMIC: exploring the world's knowledge of somatic mutations in human cancer. Nucleic Acids Res. 43, D805–D811.

7. Eberhardt, W., Doller, A., Akool, S., and Pfeilschifter, J. (2007). Modulation of mRNA stability as a novel therapeutic approach. Pharmacol. Ther. 114, 56–73.

8. Schoenberg, D.R., and Maquat, L.E. (2012). Regulation of cytoplasmic mRNA decay. Nat. Rev. Genet. 13, 246–259.

9. Castello, A., Fischer, B., Eichelbaum, K., Horos, R., Beckmann, B.M., Strein, C., Davey, N.E., Humphreys, D.T., Preiss, T., Steinmetz, L.M., et al. (2012). Insights into RNA biology from an atlas of mammalian mRNA-binding proteins. Cell 149, 1393–1406.

10. Gerstberger, S., Hafner, M., and Tuschl, T. (2014). A census of human RNA-binding proteins. Nat. Rev. Genet. 15, 829–845.

11. Dang, H., Takai, A., Forgues, M., Pomyen, Y., Mou, H., Xue, W., Ray, D., Ha, K.C.H., Morris, Q.D., Hughes, T.R., et al. (2017). Oncogenic activation of the RNA binding

protein NELFE and MYC signaling in hepatocellular carcinoma. Cancer Cell 32, 101–114.e8.

12. Yang, G., Fu, H., Zhang, J., Lu, X., Yu, F., Jin, L., Bai, L., Huang, B., Shen, L., Feng, Y., et al. (2010). RNA-binding protein quaking, a critical regulator of colon epithelial differentiation and a suppressor of colon cancer. Gastroenterology 138, 231–240.e1–5.

13. Fagoonee, S., Picco, G., Orso, F., Arrigoni, A., Longo, D.L., Forni, M., Scarfò, I., Cassenti, A., Piva, R., Cassoni, P., et al. (2017). The RNA-binding protein ESRP1 promotes human colorectal cancer progression. Oncotarget 8, 10007–10024.

14. Kumar, B., Singh, S., Skvortsova, I., and Kumar, V. (2017). Promising targets in anti-cancer drug development: recent updates. Curr. Med. Chem. 24, 4729–4752.

15. Rabik, C.A., and Dolan, M.E. (2007). Molecular mechanisms of resistance and toxicity associated with platinating agents. Cancer Treat. Rev. 33, 9–23.

16. Rivera, F., Vega-Villegas, M.E., and López-Brea, M.F. (2007). Chemotherapy of advanced gastric cancer. Cancer Treat. Rev. 33, 315–324.

17. Yang, A.D., Fan, F., Camp, E.R., van Buren, G., Liu, W., Somcio, R., Gray, M.J., Cheng, H., Hoff, P.M., and Ellis, L.M. (2006). Chronic oxaliplatin resistance induces epithelial-to-mesenchymal transition in colorectal cancer cell lines. Clin. Cancer Res. 12, 4147–4153.

18. Martin, L.P., Hamilton, T.C., and Schilder, R.J. (2008). Platinum resistance: the role of DNA repair pathways. Clin. Cancer Res. 14, 1291–1295.

19. Al-Lazikani, B., Banerji, U., and Workman, P. (2012). Combinatorial drug therapy for cancer in the post-genomic era. Nat. Biotechnol. 30, 679–692.

20. Kouyama, Y., Masuda, T., Fujii, A., Ogawa, Y., Sato, K., Tobo, T., Wakiyama, H., Yoshikawa, Y., Noda, M., Tsuruda, Y., et al. (2019). Oncogenic splicing abnormalities induced by DEAD-Box Helicase 56 amplification in colorectal cancer. Cancer Sci. 110, 3132–3144.

21. Qiao, G.J., Chen, L., Wu, J.C., and Li, Z.R. (2019). Identification of an eight-gene signature for survival prediction for patients with hepatocellular carcinoma based on integrated bioinformatics analysis. PeerJ 7, e6548.

22. Wang, K., Li, L., Fu, L., Yuan, Y., Dai, H., Zhu, T., Zhou, Y., and Yuan, F. (2019). Integrated bioinformatics analysis the function of RNA binding proteins (RBPs) and their prognostic value in breast cancer. Front. Pharmacol. 10, 140.

23. Yang, H.W., Kim, T.M., Song, S.S., Menon, L., Jiang, X., Huang, W., Black, P.M., Park, P.J., Carroll, R.S., and Johnson, M.D. (2015). A small subunit processome protein promotes cancer by altering translation. Oncogene 34, 4471–4481.

24. Subramanian, A., Tamayo, P., Mootha, V.K., Mukherjee, S., Ebert, B.L., Gillette, M.A., Paulovich, A., Pomeroy, S.L., Golub, T.R., Lander, E.S., and Mesirov, J.P. (2005). Gene set enrichment analysis: a knowledge-based approach for interpreting genome-wide expression profiles. Proc. Natl. Acad. Sci. USA 102, 15545–15550.

25. Fabregat, A., Jupe, S., Matthews, L., Sidiropoulos, K., Gillespie, M., Garapati, P., Haw, R., Jassal, B., Korninger, F., May, B., et al. (2018). The Reactome Pathway Knowledgebase. Nucleic Acids Res. 46 (D1), D649–D655.

26. He, Y., Meng, X.M., Huang, C., Wu, B.M., Zhang, L., Lv, X.W., and Li, J. (2014). Long noncoding RNAs: novel insights into hepatocelluar carcinoma. Cancer Lett. 344, 20–27.

27. Li, Y., McGrail, D.J., Xu, J., Li, J., Liu, N.N., Sun, M., Lin, R., Pancsa, R., Zhang, J., Lee, J.S., et al. (2019). MERIT: systematic analysis and characterization of mutational effect on RNA interactome topology. Hepatology 70, 532–546.

28. Chen, N., Fang, W., Lin, Z., Peng, P., Wang, J., Zhan, J., Hong, S., Huang, J., Liu, L., Sheng, J., et al. (2017). KRAS mutation-induced upregulation of PD-L1 mediates immune escape in human lung adenocarcinoma. Cancer Immunol. Immunother. 66, 1175–1187.

29. Sherwood, V. (2015). WNT signaling: an emerging mediator of cancer cell metabolism? Mol. Cell. Biol. 35, 2–10.

30. Weiske, J., Albring, K.F., and Huber, O. (2007). The tumor suppressor Fhit acts as a repressor of beta-catenin transcriptional activity. Proc. Natl. Acad. Sci. USA 104, 20344–20349.

31. Rothenberg, M.L. (2000). Efficacy of oxaliplatin in the treatment of colorectal cancer. Oncology (Williston Park) 14 (12, Suppl 11), 9–14.

32. Li, Y.E., Xiao, M., Shi, B., Yang, Y.T., Wang, D., Wang, F., Marcia, M., and Lu, Z.J. (2017). Identification of high-confidence RNA regulatory elements by combinatorial classification of RNA-protein binding sites. Genome Biol. 18, 169.

33. Yan, X., Hu, Z., Feng, Y., Hu, X., Yuan, J., Zhao, S.D., Zhang, Y., Yang, L., Shan, W., He, Q., et al. (2015). Comprehensive genomic characterization of long non-coding RNAs across human cancers. Cancer Cell 28, 529–540.

34. Neelamraju, Y., Gonzalez-Perez, A., Bhat-Nakshatri, P., Nakshatri, H., and Janga, S.C. (2018). Mutational landscape of RNA-binding proteins in human cancers. RNA Biol. 15, 115–129.

35. St Laurent, G., Wahlestedt, C., and Kapranov, P. (2015). The landscape of long non-coding RNA classification. Trends Genet. 31, 239–251.

36. Marchese, F.P., Raimondi, I., and Huarte, M. (2017). The multidimensional mechanisms of long noncoding RNA function. Genome Biol. 18, 206.

37. Quinn, J.J., and Chang, H.Y. (2016). Unique features of long non-coding RNA biogenesis and function. Nat. Rev. Genet. 17, 47–62.

38. Ferrè, F., Colantoni, A., and Helmer-Citterich, M. (2016). Revealing protein-lncRNA interaction. Brief. Bioinform. 17, 106–116.

39. Dang, C.V. (2012). MYC on the path to cancer. Cell 149, 22–35.

40. Kress, T.R., Sabò, A., and Amati, B. (2015). MYC: connecting selective transcriptional control to global RNA production. Nat. Rev. Cancer 15, 593–607.

41. Xiang, J.F., Yin, Q.F., Chen, T., Zhang, Y., Zhang, X.O., Wu, Z., Zhang, S., Wang, H.B., Ge, J., Lu, X., et al. (2014). Human colorectal cancer-specific CCAT1-L lncRNA regulates long-range chromatin interactions at the MYC locus. Cell Res. 24, 513–531.

42. Hung, C.L., Wang, L.Y., Yu, Y.L., Chen, H.W., Srivastava, S., Petrovics, G., and Kung, H.J. (2014). A long noncoding RNA connects c-Myc to tumor metabolism. Proc. Natl. Acad. Sci. USA 111, 18697–18702.

43. Yang, F., Xue, X., Zheng, L., Bi, J., Zhou, Y., Zhi, K., Gu, Y., and Fang, G. (2014). Long non-coding RNA GHET1 promotes gastric carcinoma cell proliferation by increasing c-Myc mRNA stability. FEBS J. 281, 802–813.

44. Wang, Z., Yang, B., Zhang, M., Guo, W., Wu, Z., Wang, Y., Jia, L., Li, S., Xie, W., and Yang, D.; Cancer Genome Atlas Research Network (2018). lncRNA epigenetic landscape analysis identifies EPIC1 as an oncogenic lncRNA that interacts with MYC and promotes cell-cycle progression in cancer. Cancer Cell 33, 706–720.e9.

45. Herranz, D., Ambesi-Impiombato, A., Palomero, T., Schnell, S.A., Belver, L., Wendorff, A.A., Xu, L., Castillo-Martin, M., Llobet-Navás, D., Cordon-Cardo, C., et al. (2014). A NOTCH1-driven MYC enhancer promotes T cell development, transformation and acute lymphoblastic leukemia. Nat. Med. 20, 1130–1137.

46. Zhang, X., Choi, P.S., Francis, J.M., Imielinski, M., Watanabe, H., Cherniack, A.D., and Meyerson, M. (2016). Identification of focally amplified lineage-specific super-enhancers in human epithelial cancers. Nat. Genet. 48, 176–182.

47. Martinez-Balibrea, E., Martínez-Cardús, A., Ginés, A., Ruiz de Porras, V., Moutinho, C., Layos, L., Manzano, J.L., Bugés, C., Bystrup, S., Esteller, M., and Abad, A. (2015). Tumor-related molecular mechanisms of oxaliplatin resistance. Mol. Cancer Ther. 14, 1767–1776.

48. Kelland, L. (2007). The resurgence of platinum-based cancer chemotherapy. Nat. Rev. Cancer 7, 573–584.

49. Hong, S. (2017). RNA binding protein as an emerging therapeutic target for cancer prevention and treatment. J. Cancer Prev. 22, 203–210.

50. Hsieh, A.C., and Ruggero, D. (2010). Targeting eukaryotic translation initiation factor 4E (eIF4E) in cancer. Clin. Cancer Res. 16, 4914–4920.

51. Huang, Y.H., Peng, W., Furuuchi, N., Gerhart, J., Rhodes, K., Mukherjee, N., Jimbo, M., Gonye, G.E., Brody, J.R., Getts, R.C., and Sawicki, J.A. (2016). Delivery of therapeutics targeting the mRNA-binding protein HuR using 3DNA nanocarriers suppresses ovarian tumor growth. Cancer Res. 76, 1549–1559.

52. Weinstein, J.N., Collisson, E.A., Mills, G.B., Shaw, K.R., Ozenberger, B.A., Ellrott, K., Shmulevich, I., Sander, C., and Stuart, J.M.; Cancer Genome Atlas Research Network

(2013). The Cancer Genome Atlas Pan-Cancer analysis project. Nat. Genet. *45*, 1113–1120.

53. Barretina, J., Caponigro, G., Stransky, N., Venkatesan, K., Margolin, A.A., Kim, S., Wilson, C.J., Lehár, J., Kryukov, G.V., Sonkin, D., et al. (2012). The Cancer Cell Line Encyclopedia enables predictive modelling of anticancer drug sensitivity. Nature *483*, 603–607.

54. Cancer Genome Atlas, N.; Cancer Genome Atlas Network (2012). Comprehensive molecular characterization of human colon and rectal cancer. Nature *487*, 330–337.

55. Mootha, V.K., Lindgren, C.M., Eriksson, K.F., Subramanian, A., Sihag, S., Lehar, J., Puigserver, P., Carlsson, E., Ridderstråle, M., Laurila, E., et al. (2003). PGC-1α-responsive genes involved in oxidative phosphorylation are coordinately downre-gulated in human diabetes. Nat. Genet. *34*, 267–273.

56. Gao, B., Huang, Q., and Baudis, M. (2018). segment_liftover : a Python tool to convert segments between genome assemblies. F1000Res. *7*, 319.

57. Quinlan, A.R., and Hall, I.M. (2010). BEDTools: a flexible suite of utilities for comparing genomic features. Bioinformatics *26*, 841–842.

Supplemental Information

RBP EIF2S2 Promotes Tumorigenesis and

Progression by Regulating MYC-Mediated

Inhibition via FHIT-Related Enhancers

Jiwei Zhang, Shengli Li, Ling Zhang, Juan Xu, Mingxu Song, Tingting Shao, Zhaohui Huang, and Yongsheng Li

Supporting materials and methods

RNA pull-down assays and mass spectrometry analyses

LINC01600 or antisense-LINC01600 RNAs were transcribed and labelled by the Biotin RNA Labeling Mix (Roche, USA), treated with RNase-free DNase I (Takara, Japan) and purified with an RNeasy Mini Kit (QIAGEN, USA). Briefly, LINC01600 sequence was in vitro transcribed with biotin RNA-labeling mix and T7 RNA polymerase (Invitrogen) according to the manufacturer's instructions. The pre-treated biotinylated RNAs were incubated with 1mg protein extracts of HCT-116 cells at 4 °C for 1h, gently mixed with 40µl washed streptavidin beads (Invitrogen, USA) and incubated on a rotator overnight. The beads were washed briefly five times in 1× washing buffer (5mM Tris-HCl, 1M NaCl, 0.5mM EDTA, and 0.005% Tween 20). The proteins were precipitated and diluted in 60µl protein lysis buffer, separated by gel electrophoresis and visualized by silver staining. Specific bands were excised for proteomics screening by mass spectrometry analysis (Shanghai Applied Protein Technology, Shanghai, China).

RNA Immunoprecipitation assay

RNA Immunoprecipitation (RIP) assays were performed using the Magna RIP RNA-Binding Protein Immunoprecipitation Kit (Millipore). Briefly, cells growing in 15cm-dishes were lysed in 1.2ml of lysis buffer containing protease inhibitors and RNase Inhibitor (Thermo Fisher Scientific Inc., Rockford, IL, USA) and centrifuged at 12,000 r.p.m. for 30min. The supernatants were incubated with Protein G Dynabeads (Thermo Fisher Scientific, Carlsbad, California, USA), which were incubated with the indicated antibodies for 12h at 4°C with gentle rotation. The beads were washed thrice with wash buffer containing RNase inhibitor and then twice with PBS containing RNase inhibitor. The RNA was extracted using the Total RNA isolation kit (Thermo Fisher Scientific Inc), and qRT-PCR was performed as described in Supplemental Materials. For the RIP assays of deletion mutants, 5p mol plasmids with FLAG- or HA-tagged full-length and truncated EIF2S2, MYC were transiently transfected into HCT-116 cells, and the cell lysates were immunoprecipitated with indicated antibodies.

DNA and RNA isolation

Genomic DNA was isolated using the General AllgGen Kit (Cwbio, China) according to the manufacturer's protocol. Total RNA was extracted using RNAiso reagent (Takara, Japan). The concentrations of DNA and RNA were determined using NanoDrop 2000 (Thermo, USA). Complementary DNA (cDNA) was synthesized using the PrimeScript RT reagent kit (TaKaRa,

Japan). qRT-PCR analyses were conducted to quantitate the relative mRNA expression using SYBR Premix Ex Taq (TaKaRa), with β-actin as an internal control. qRT-PCR assays were carried out using TaqMan probes (Applied Biosystems, USA). The reactions were incubated in 96- or 384-well optical plates at 95°C for 10 min, followed by 40 cycles of 95°C for 15 s and 60°C for 1 min. After the reactions, the cycle threshold (Ct) data were determined using default threshold settings, and the mean Ct was determined from the duplicate PCRs. A comparative ΔCt method was used to compare each condition with controls, and the values are expressed as 2−△Ct. The relative levels of mRNAs were normalized to U6, a ubiquitously expressed small nuclear RNA. All the primers were listed in Table S2.

Western blotting

Total protein was separated by 8% (or 10%) sodium dodecyl sulfate polyacrylamide gel electrophoresis and transferred to a PVDF membrane. After blocking with non-fat milk, the polyvinylidene difluoride membrane was incubated with a rabbit anti-human NOTCH1 antibody (1:1000, 20687-1-AP, Proteintech, USA) or a mouse anti-β-actin antibody (1:1000, AA128, Beyotime, China).

Northern blot

We used a NorthernMax Kit from Ambion (Thermo Fisher Scientific,Carlsbad, California, USA) and DIG Northern starter Kit (Roche, Indianapolis,Indiana, USA) with Digoxin-labelled RNA probes to detect LINC01600 in the HCT-116 and LoVo cells. Approximately 10μg of enriched polyA + RNA was loaded per lane for northern blot analysis, according to the manufacturer's instructions.

5′ and 3′ RACE assay

We used 5′ and 3′ RACE to determine the transcriptional initiation and termination sites of LINC01600 with a SMARTer RACE cDNA Amplification kit (Clontech, California, USA), according to manufacturer's instructions. The sequences for the gene-specific PCR primers used for 5′ and 3′RACE analysis are given in Table S2.

Subcellular fractionation

Cytoplasmic and nuclear fractions of HCT-116 cells were prepared and collected according to the instructions of the Nuclear/Cytoplasmic Isolation kit (Thermo Fisher Scientific, Carlsbad, California, USA). β-actin was used as the cytoplasmic endogenous control. U2 small nuclear RNA was used as the nuclear endogenous control.

Cell proliferation and colony formation assays

The cells were seeded in 96-well flat-bottomed plates, with each well containing 1500 cells in 100μl of cell suspension. After a certain time in culture, cell proliferation was quantified using the Cell Counting Kit-8 (CCK8; Dojindo Laboratories, Japan) according to the manufacturer's instructions. For the colony formation assays, 1000 cells of HCT-116, SNU-449, MGC-803 and 1500 cells of SGC-7901 and Huh-7 cells were plated into each well of 6-well plates and incubated in medium containing 10% FBS for 15 days. The colonies were fixed with methanol and stained with 0.1% crystal violet in 20% methanol for 20 min. The number of colonies containing more than about 30 cells was counted using an inverted microscope.

Invasion and migration assays

Invasion assays were performed in Millicell chambers in triplicate. The 8-μm pore inserts were coated with 30μg of Matrigel (BD Biosciences, Franklin Lakes, New Jersey, USA). The migration assay was conducted similarly, without coating filters with Matrigel. The cells (3×10^4) were added to the coated filters in serum-free medium. We added medium containing 10% FBS to the lower chambers as a chemoattractant. After 24 h at 37 °C in an incubator at 5% CO2, cells that migrated through the filters were fixed with methanol and stained with crystal violet. Cell numbers were counted in five random fields.

Luciferase assay

Approximately 5,000 HEK-293T cells or 10,000 CRC (HCT-116, LoVo) cells per well were plated into 96-well plates and were co-transfected with 50 nmol/L of siRNA (or NC), 50 ng of the luciferase reporter, and 10 ng of the pRL-CMV Renilla luciferase reporter using 0.5 μL Lipofectamine 2000 (Invitrogen, USA) per well. After 48-h of transfection, the luciferase activities were quantified using a dual-luciferase reporter assay (Promega, USA).

In vivo **assays**

Female athymic BALB/c nude mice, aged 4–5 weeks old, purchased from the Experimental Animal Center of Shanghai Cancer Institute (Shanghai, China). Mice (10 in each group) were injected subcutaneously with 0.2 ml of cell suspension containing 5×10^5 cells (pWPXL-VECTOR and pWPXL-EIF2S2 stable LoVo cell line) in the right axilla. Tumor growth rates were monitored. When a tumor was palpable, it was measured every other day, and its volume was calculated according to the formula volume = length × width^{2}x0.5. Sample size was not predetermined for these experiments. In addition, an orthotopic mouse model was used to

evaluate the effect of EIF2S2 on hepatic metastasis. Briefly, 2×10^6 LoVo cells stably expressing EIF2S2 were injected into the submucosal tissue of cecum of an athymic male BALB/c nude mouse at 4-5 weeks of age (n=10 for each group). The number of metastatic foci in the liver, lung and intestine were determined using the hematoxylin eosin (H&E) (Beyotime Biotechnology) staining in tissue sections under a binocular microscope (Leica, Wetzlar Lottehaus, Germany). All experiments were performed in accordance with relevant institutional and national guidelines and regulations of Shanghai Medical Experimental Animal Care Commission.

RNA interference and generation of lentivirus particles

The sequences of small interfering RNA (siRNA) oligonucleotides targeting EIF2S2, LINC01600, MYC,FHIT and the negative control siRNA were purchased from RiboBio (RiboBio Biotechnology, Guangzhou, China). Transfections with siRNA (50 nM) were performed with Lipofectamine 2000. The human EIF2S2 sequence was cloned from HCT-116 cell cDNA and cloned into lentivirus expression vector pWPXL to generate pWPXL-EIF2S2 cells. The LINC01600 and FHIT expression vectors were constructed by inserting the respective sequences into pWPXL vector to generate pWPXL-LINC01600 and pWPXL-FHIT, respectively. The HEK293T cells were transfected with pWPXLEIF2S2, pWPXL-MYC, pWPXL-LINC01600 or pWPXL-FHIT, with the packaging and envelope plasmids psPAX2 and pMD2.G, respectively (gifts from Dr. Didier), using Lipofectamine 2000 (Invitrogen) according to the manufacturer's instructions.

Immunoblotting analysis

CRC Cells (5×10^6) were lysed for 30 min with lysis buffer (Beyotime Biotechnology) containing protease inhibitors (Roche, Indianapolis, IN, USA). The protein concentrations were determined by the BCA method (Pierce, Thermo Fisher Scientific Inc., Rockford, IL, USA). After centrifugation at 16,400×g for 15 min at 4 °C, the samples were resolved by SDS/PAGE, transferred to PVDF membranes (Immobilon-P membrane, Millipore, Massachusetts, USA), and analyzed by immune blotting using HRP-conjugated secondary antibodies. The membranes were blocked with 5% (wt/vol) skimmed milk in TBS plus Tween 20 at 4 °C overnight before probing with antibodies. Information on the antibodies are provided Supplementary Table 2. An enhanced chemiluminescent (ECL) chromogenic substrate was used to visualize the bands (Pierce). Visualization was performed using the Enhanced Chemiluminescence Plus Western Blotting Detection System (GE Healthcare, Connecticut, USA) and LAS-4000EPUV mini Luminescent Image Analyzer (GE Healthcare).

Immunohistochemistry

The expression levels of EIF2S2 and MYC protein were determined by immunohistochemistry (IHC) analysis using colorectal cancer tissue arrays constructed previously. IHC staining was performed on 4-mm sections of paraffin-embedded tissue samples. Briefly, the slides were incubated with an anti-EIF2S2 and anti-MYC antibody (CST, 1:200) at 4°C overnight. The subsequent steps were performed using the GTVision III Detection System/Mo&Rb (GeneTech, China).

***In vitro* cellular IC50 assays**

Vector and pWPXL-EIF2S2 LoVo cells and siNC, siEIF2S2 HCT-116 were seeded in 96-well flat-bottomed plates, with each well containing 5000 cells in 100 μl of cell suspension to determine the concentration that causes 50% inhibition of cell viability. According to the recommended concentrations of Oxaliplation, we performed 8 concentration gradients. After 72 h in culture, the cell viability was measured using Cell Counting Kit-8 (CCK-8) assays (Dojindo). Each experiment with six replicates was repeated three times.

Processing EIF2S2 knockdown RNA-Seq data

The raw sequencing reads were first processed to trim adapter sequences and low-quality bases by Trimmomatic (Version 0.36)[1]. The parameters was "ILLUMINACLIP: 'Aapter':2:30:10' LEADING:3 TRAILING:3 SLIDINGWINDOW:4:15 MINLEN:36". All filtered reads were aligned to the human reference genome (GRch38) by using the splice-aware aligner HISAT2 with default settings[2]. Next, the alignments were subjected to StingTie[3] program to calculate the gene expression in FPKM units (FPKM = Fragments Per Kilobase of transcript per Million mapped reads). Furthermore, the lncRNAs annotated in GENCODE v28 were adopted to extract lncRNA expression profiles.

Gene set enrichment analysis

To identify the pathways potentially regulated by EIF2S2, we first calculated the expression correlation coefficient for each gene with EIF2S2. All protein coding genes were ranked based on the correlation coefficient. Next, we calculated the enrichment score (*ES*) based on the GSEA. If there were *N* genes in the ranked gene list $L = \{g_1, g_2, g_3, …, g_N\}$, the ranked score is $\mathrm{RS}(g_j) = r_j$. We first calculated the fraction of gene in pathway H ("hits") weighted by their rank score and the fraction of genes not in S ("misses") present up to a given position *i* in *L*.

$$P_{hit}(H, i) = \sum_{\substack{g_i \in H \\ j \leq i}} \frac{|r_j|^p}{N_R}, where\ N_R = \sum_{g_i \in H} |r_j|^p$$

$$P_{miss}(H, i) = \sum_{\substack{g_{j \notin H} \\ j \leq i}} \frac{1}{(N - N_I)}$$

The ES score was the maximum deviation from zero of $P_{hit} - P_{miss}$. Moreover, a p-value was calculated for each pathway that includes N_I of genes.

$$p(ES(N, N_I) < ES_{ik}) = \sum_{q=-\infty}^{\infty} (-1)^q \exp\left(-2q^2 ES_{ik}{}^2 n\right),$$

$$n = \frac{(N - N_I)N_I}{N}$$

Where ES_{ik} is the enrichment score for functional pathway k, N is the number of genes in the ranked list, and N_I the number of genes in the specific functional pathway. P-values were adjusted by false discovery rate (FDR).

References

1. Bolger, AM, Lohse, M, and Usadel, B (2014). Trimmomatic: a flexible trimmer for Illumina sequence data. *Bioinformatics* **30**: 2114-2120.
2. Kim, D, Langmead, B, and Salzberg, SL (2015). HISAT: a fast spliced aligner with low memory requirements. *Nature methods* **12**: 357-360.
3. Pertea, M, Pertea, GM, Antonescu, CM, Chang, TC, Mendell, JT, and Salzberg, SL (2015). StringTie enables improved reconstruction of a transcriptome from RNA-seq reads. *Nature biotechnology* **33**: 290-295.

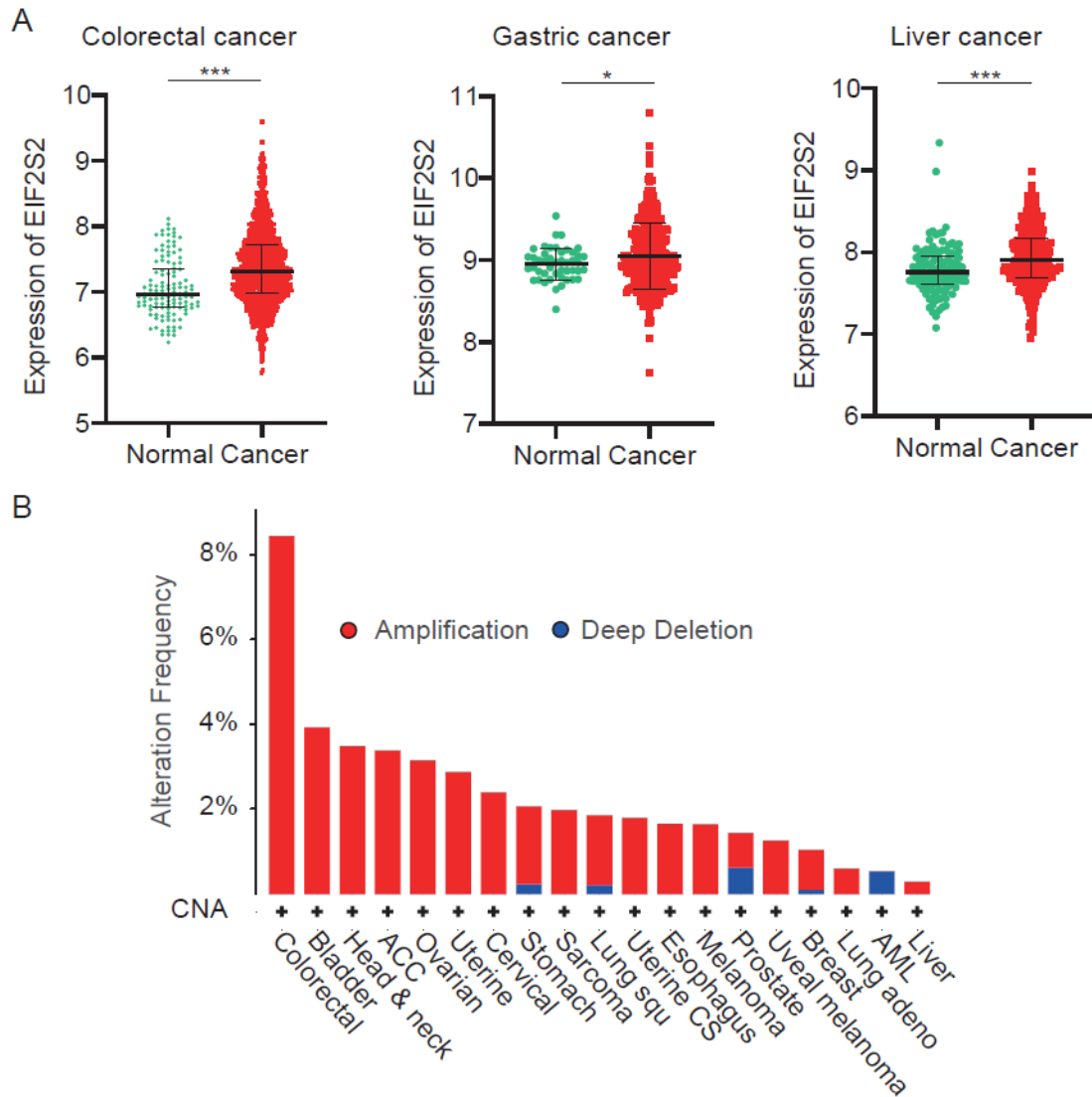**Supplementary figures**

A

B

Figure S1. The expression and copy number variation of EIF2S2 in independent data. (A) The expression of EIF2S2 in normal and cancer patients across three cancer types. (B) The copy number alteration frequency of EIF2S2 across different cancer types in TCGA project.
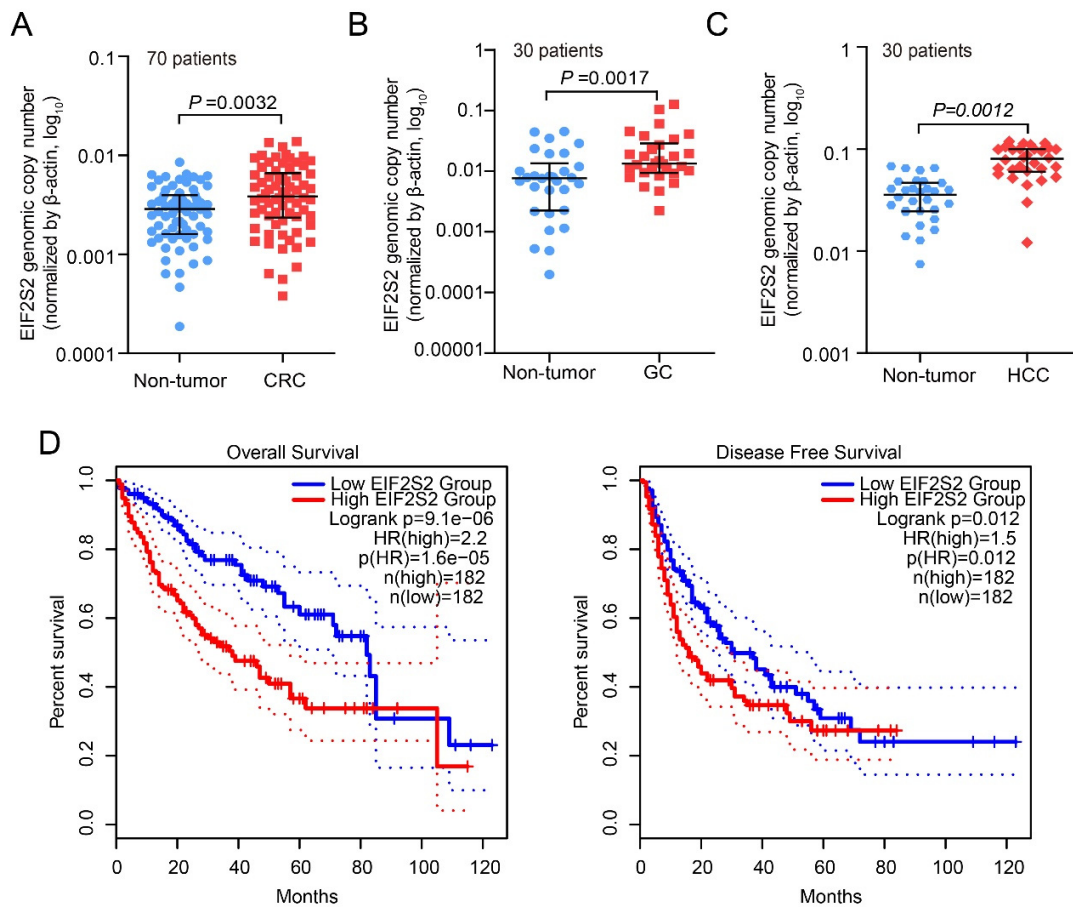
Figure S2. The copy number and clinical association of EIF2S2 in cancer.

(A) The copy numbers of EIF2S2 in 70 pairs of CRC tissues and adjacent normal tissues quantified by q-PCR. (B) The copy numbers of EIF2S2 in 30 pairs of GC tissues and adjacent normal tissues quantified by q-PCR. (C) The copy numbers of EIF2S2 in 30 pairs of HCC tissues and adjacent normal tissues quantified by q-PCR. (D) Kaplan–Meier analyses of the correlation between EIF2S2 RNA levels and the overall survival (left panel) and disease free survival analysis in HCC (right panel).
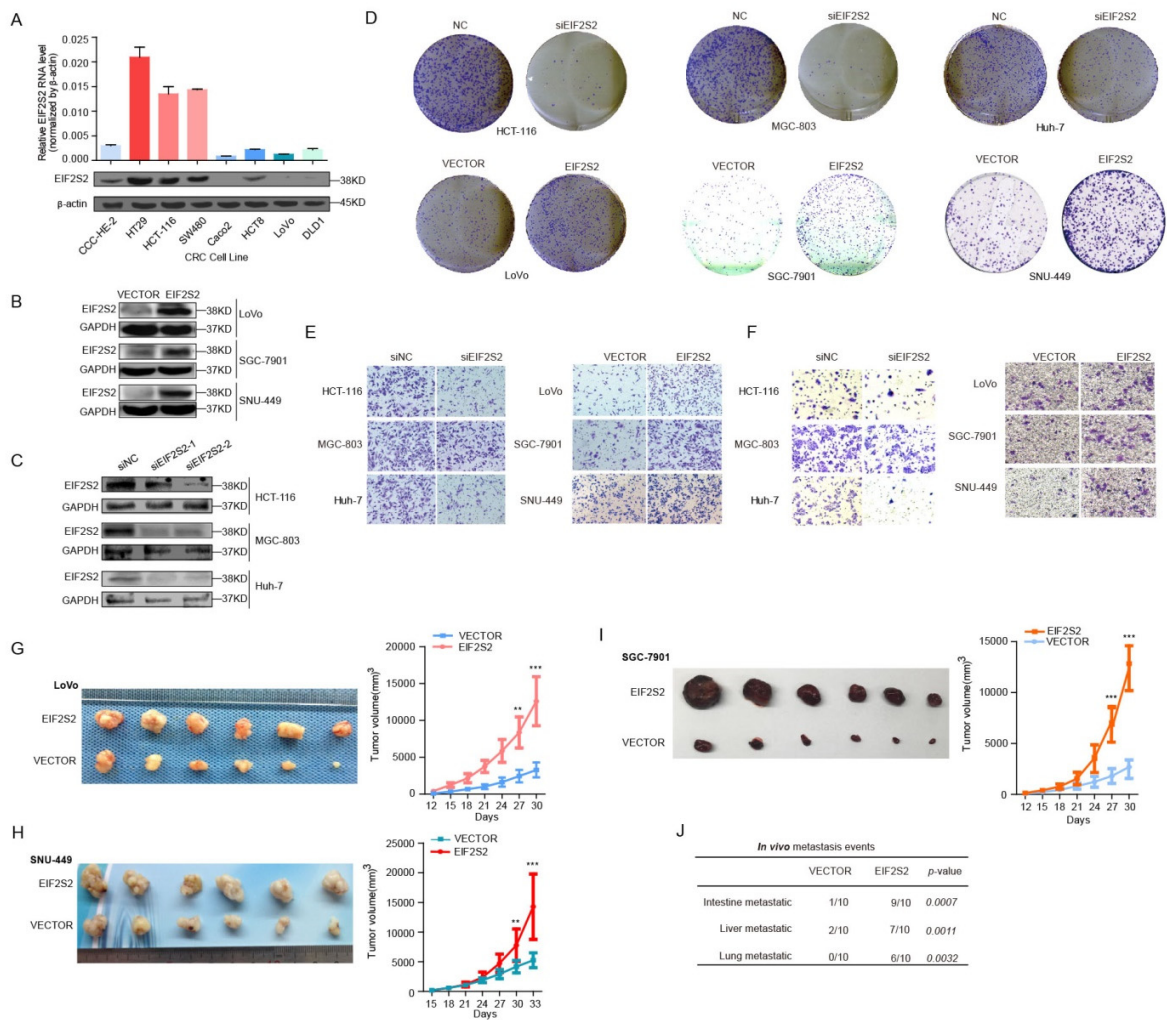
Figure S3. Oncogenetic functions of EIF2S2 in cancer.

(A) RNA levels of EIF2S2 in eight CRC cell lines (top panel), and protein levels of EIF2S2 in eight CRC cell lines (bottom panel). (B) The activation of EIF2S2 by pWPXL-EIF2S2 activation in the LoVo, SGC-7901 and SNU-449 cell lines. (C) The knockout efficiency of EIF2S2 by siRNA in HCT-116, MGC-803 and Huh-7 cell lines. (D) Representative images of colony formation assays in siEIF2S2 or pWPXL-EIF2S2 cancer cell lines. (E) and (F) Representative images of transwell migration and invasion assays for HCT-116 and MGC-803 and Huh-7 cells infected with the siEIF2S2 or the siNC (400×magnification). (G)-(I) Document planes of nude mouse models bearing subcutaneous tumor xenografts from pWPXL-EIF2S2 cells or vector in cell lines. (J) In vivo metastatic events in LoVo cells infected with the lentivirus expressing EIF2S2 or the control.
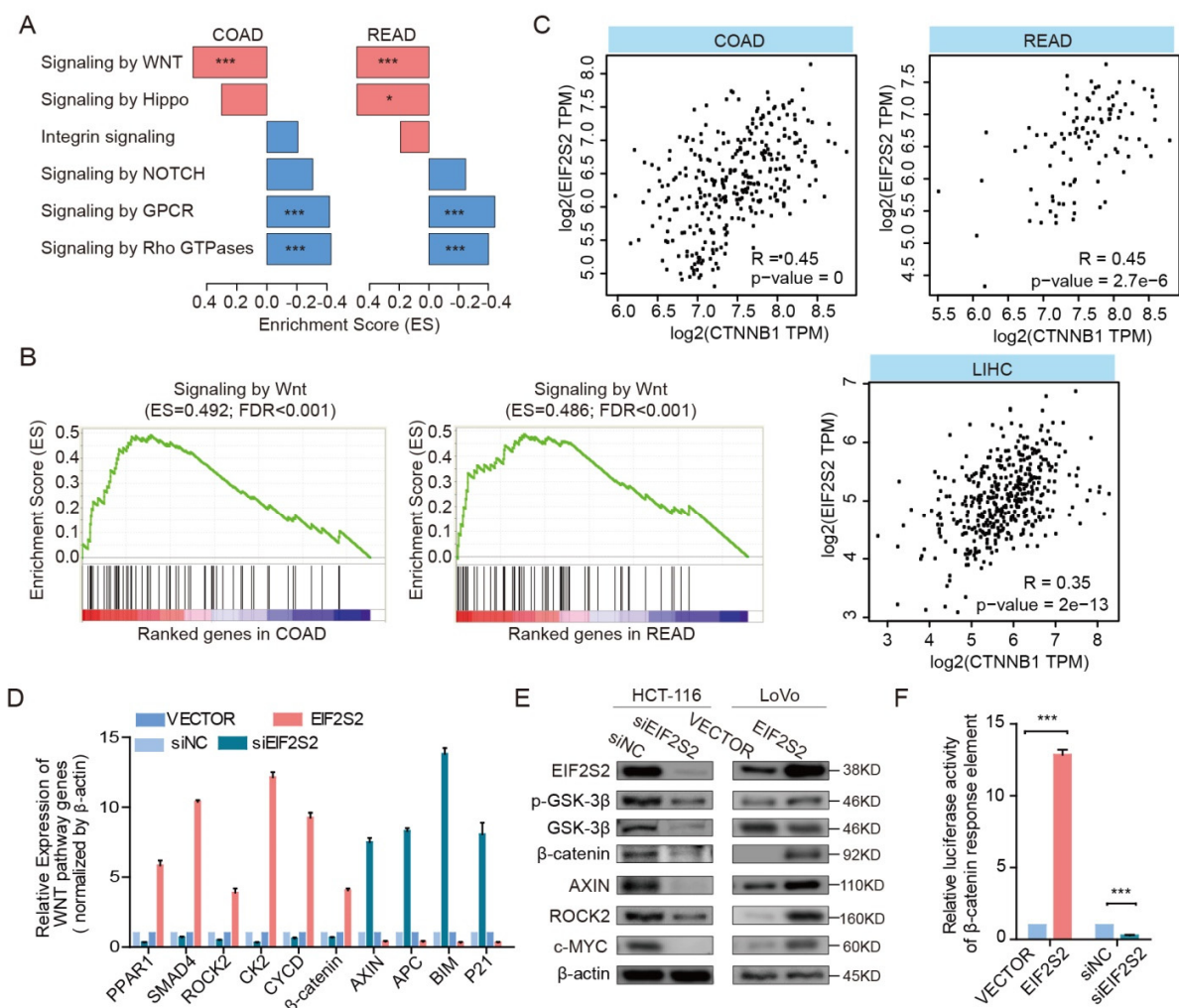
Figure S4. EIF2S2 perturbs Wnt signaling Pathway involved in tumor cell proliferation and metastasis.

(A) The signaling pathways enriched by the genes that co-expressed with EIF2S2. Left panel for COAD and right panel for READ. Red for pathways enriched by positively co-expressed genes and blue for negatively co-expressed genes. (B) GSEA enrichment plots of co-expressed genes with EIF2S2 belonging to the Wnt signaling pathway. The bar-code plot indicates the position of the genes on the expression data rank-sorted by its association with EIF2S2, with red and blue colors indicating positively and negatively co-expressed genes. (C) The scatter plots of the expression of EIF2S2 and CTNNB1 in COAD, READ and LIHC cancers. (D) The mRNA levels of Wnt signaling pathway genes in LoVo cells infected with lentivirus expressing EIF2S2 or transfected with EIF2S2 siRNAs. (E) The protein levels of Wnt signaling pathway genes in LoVo cells infected with lentivirus expressing EIF2S2 or transfected with EIF2S2 siRNAs. (F) Luciferase assays for CRC cells infected with lentivirus expressing EIF2S2 or transfected with EIF2S2 siRNAs. Values are expressed as mean±SEM (n=3). ***p<0.001, Wilcoxon signed-ranks test.
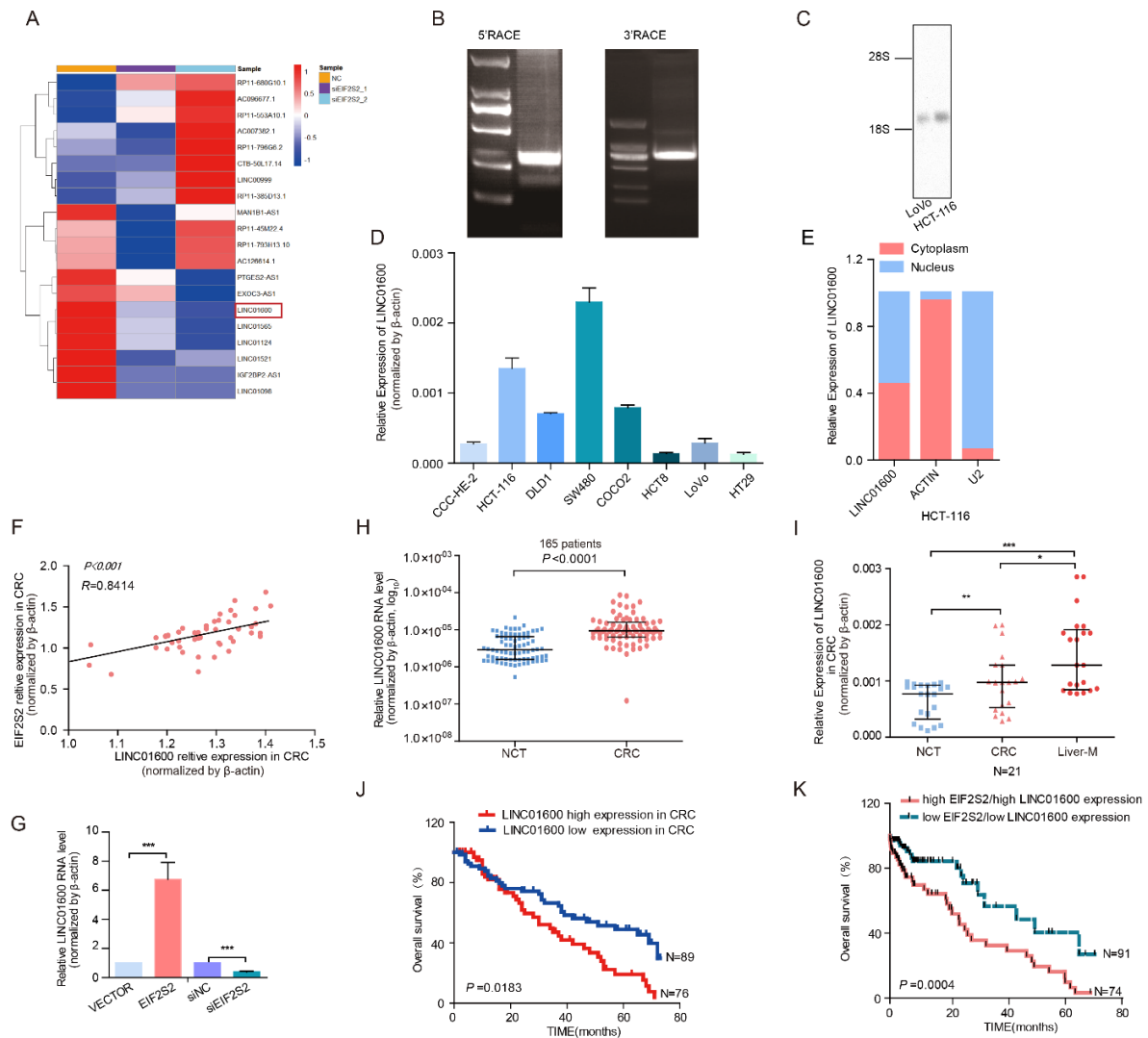
Figure S5. LINC01600 is overexpression in CRC and correlated with patient survival.

(A) Heat map of expression of lincRNAs between HCT-116 cells transfected with EIF2S2 siRNAs or control. (B) Representative images of LINC01600 PCR products from the 5' RACE and 3' RACE. (C) Northern-blotting for LINC01600 in LoVo and HCT-116. (D) The RNA levels of LINC01600 in eight CRC cell lines. (E) The distribution of LINC01600 RNA in HCT-116 cells (cytoplasmic, magenta; nuclear, spearmint). β-actin served as cytoplasmic internal control. U2 served as nuclear internal control. (F) Expression correlation of EIF2S2 and LINC01600 in CRC. (G) Relative expression of LINC01600 in EIF2S2 over-expressing and knockdown cell lines. (H) Relative expression of LINC01600 in 165 CRC patients and adjacent normal control. (I) Relative expression of LINC01600 in normal controls, cancer and liver metastatic patients. (J)

Kaplan–Meier analyses of the correlation between LINC01600 RNA levels and the overall survival in 165 patients with CRC. Patients were stratified for the analysis by the median expression of LINC01600 in CRC patients. (K) Combined influence of EIF2S2 and LINC01600 on the patient survival. The patients with high EIF2S2 expression and high LINC01600 expression showed significantly optimal survival.
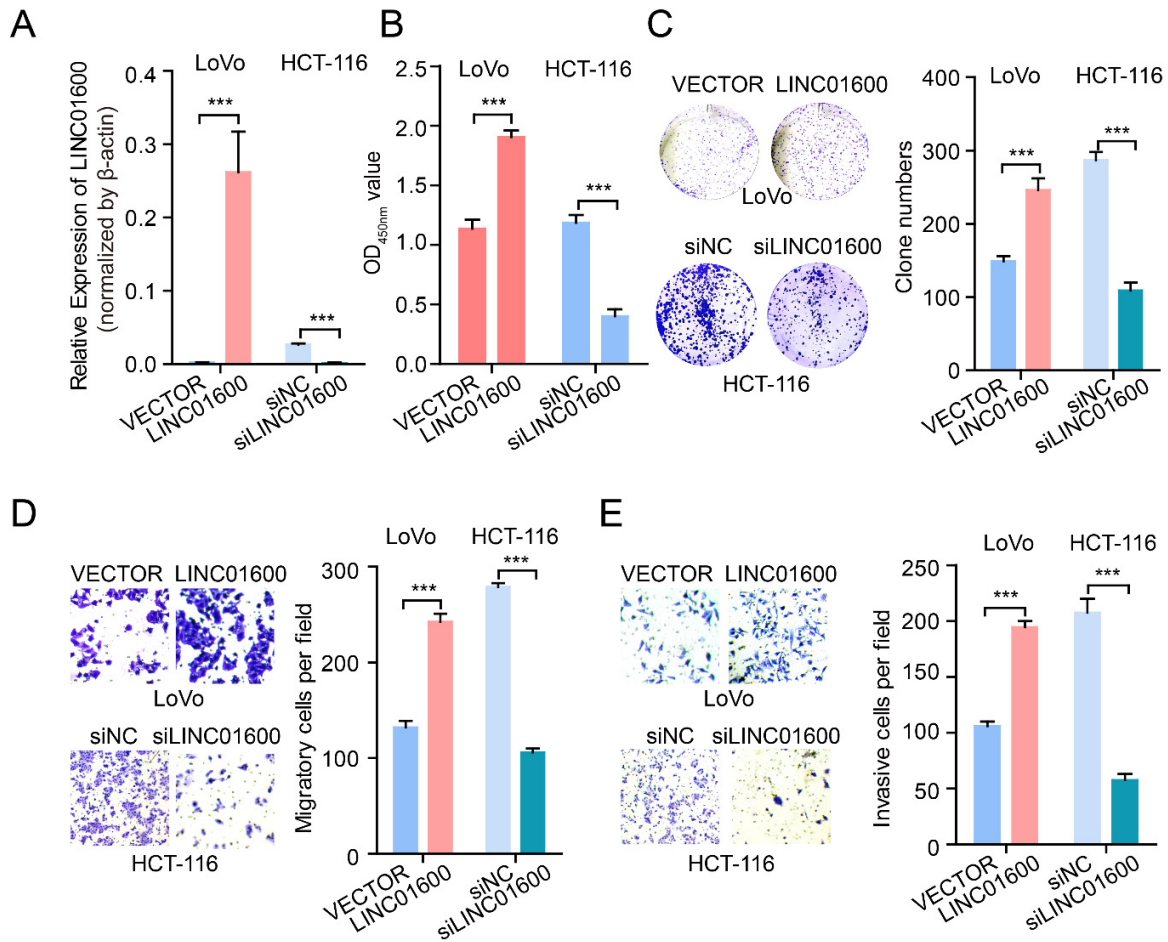

Figure S6. LINC01600 promotes CRC cell proliferation and metastasis in vitro.

(A) The activation of LINC01600 by pWPXL-LINC01600 in the LoVo, and the knockout efficiency of LINC01600 by siRNA in HCT-116 cells. (B)-(E) CCK-8 assays (B), colony formation assays (C), trans-well migration (D) and invasion (E) assays in stable pWPXL-LINC1600 LoVo and siLINC01600 HCT-116 cells. Values are represented as mean+standard error of the mean (SEM), n=3. ***P < 0.001, Wilcoxon signed-ranks test.
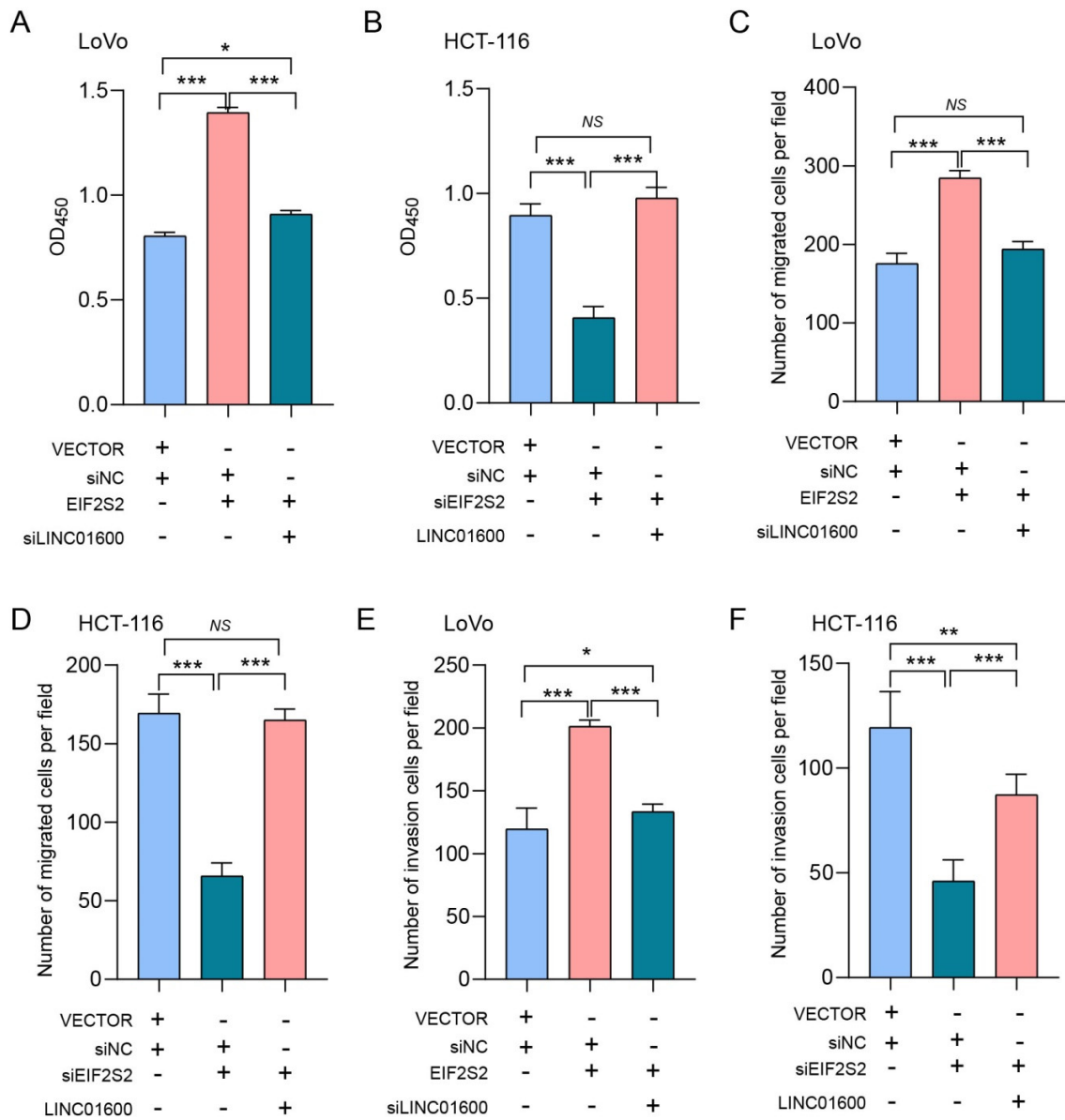
Figure S7. LINC01600 reverse the effects of EIF2S2 on cell proliferation, migration and invasion. (A) and (B), Cell proliferation. (C) and (D), Number of migrated cells per fileld. (E) and (F), Number of invasion cells per field.
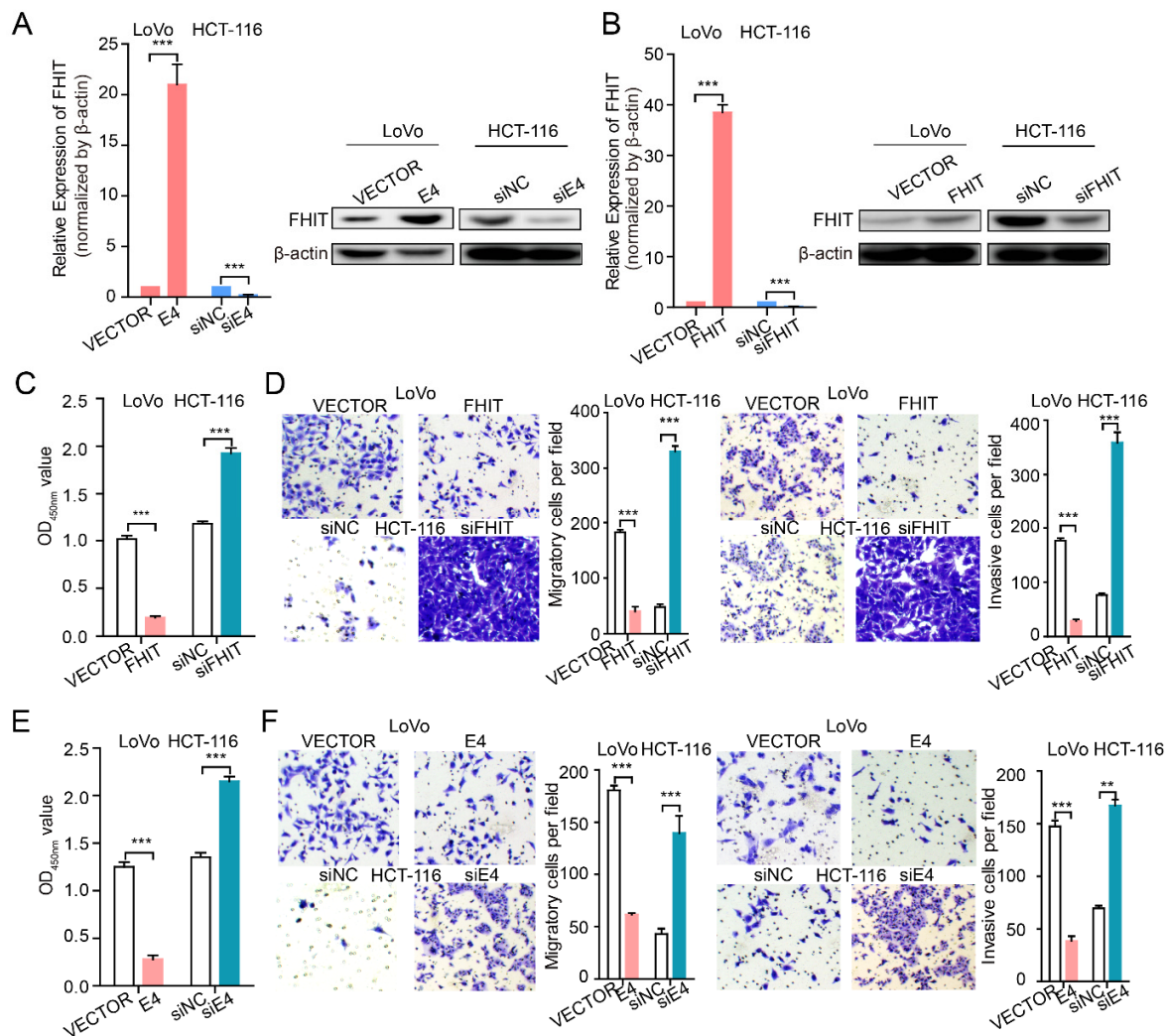
Figure S8. Enhancer E4 and FHIT function in CRC cell proliferation and metastasis in vitro.

(A) qPCR assays measuring FHIT RNA expression by inducing or repressing enhancer activity of E4 in LoVo and HCT-116 (left panels). Immunoblotting analysis FHIT protein expression affected by the enhancer activity of E4 in LoVo and HCT-116 (right panels). (B) qPCR assays measuring the activation of FHIT by pWPXL-FHIT in LoVo, and the knockout efficiency of FHIT by siRNA in HCT-116 cells (left panels). Immunoblotting analysis FHIT protein activation by pWPXL-FHIT in the LoVo, and the knockout efficiency of FHIT by siRNA in HCT-116 cells (right panels). (C) and (D) CCK-8 assays (C), trans-well migration (left panels in D) and invasion (right panels in D) assays in stable pWPXL-FHIT LoVo and siFHIT in HCT-116 cells. (E) and (F), CCK-8 assays (E), trans-well migration (left panels in F) and invasion (right panels in F) assays in stable expressing E4 in LoVo and knock down E4 in HCT-116 cells.
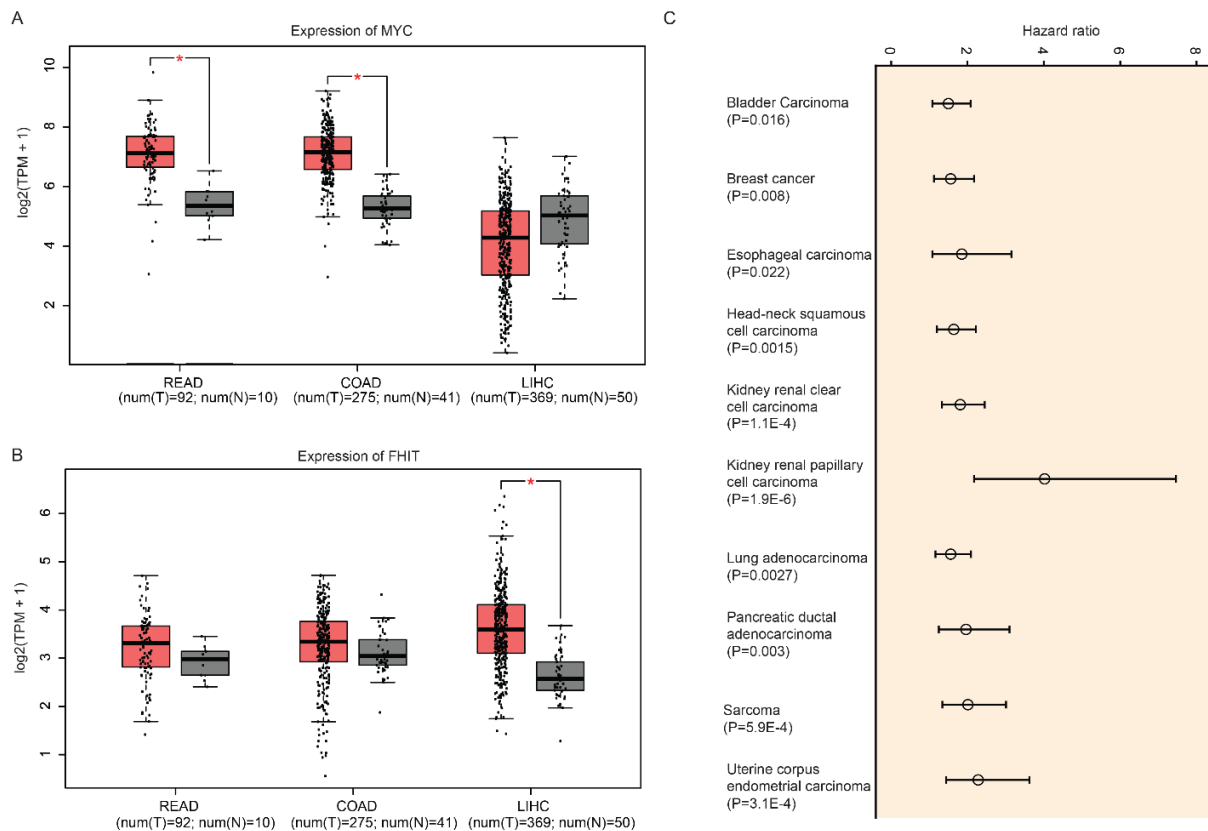
Figure S9. Expression of MYC and FHIT in cancer and clinical association of EIF2S2 across cancer types.

(A) The boxplots show the expression distribution of MYC in READ, COAD and LIHC. (B) The boxplots show the expression distribution of FHIT in READ, COAD and LIHC. (C) The hazard ratio distribution of the association between expression of EIF2S2 and patients' survival across cancer types. The log-rank p-values are shown at the bottom of each cancer type. The error bars showing the 95% confidence level of hazard ratio (HR).

Table S1. Number of cancer types and literature for RBPs. (Table S1.xls)
Table S2. Resource and primers used in this study.

REAGENT or RESOURCE	SOURCE		DENTIFIER
Antibodies			
EIF2S2	Abcam		ab86105
Phospho-GSK3β	Cell Signaling Technology		#5558
GSK3β	Cell Signaling Technology		#5676
β-catenin	Abcam		ab16051
AXIN	Cell Signaling Technology		#2521
ROCK2	Cell Signaling Technology		#9029
c-MYC	Cell Signaling Technology		#5605
β-actin	Cell Signaling Technology		#5125
GAPDH	Cell Signaling Technology		#3683
FHIT	Abcam		ab180806
siRNA sequences			
siEIF2S2	This study		AAGTCGTCCGAGTAGGAACCA
siLINC01600-1	This study		AACGTGGTGGCATCTGCTTGTGG
siLINC01600-2	This study		AAACGGGGTGGCATCCGCTC
siMYC-1	This study		GGTGTGACCGCAACGTAGGA
siMYC-2	This study		ATATCCTCGCTGGGCGCCGG
siMYC-3	This study		AACGTTGAGGGGCATCGTCG
siFHIT-1	This study		TTCTAGGATGGCCCCGAAGC
Cell Lines			
HEK-293T	This study	ATCC	
MGC-803	This study	Shanghai Meixuan	
SGC-7901	This study	Shanghai Meixuan	
LoVo	This study	ATCC	
Caco2	This study	ATCC	
HT29	This study	ATCC	
HCT8	This study	ATCC	
HCT116	This study	ATCC	
CCH-HE-2	This study	ATCC	
DLD1	This study	ATCC	
SW480	This study	ATCC	
Hu-7	This study	Japanese Collection of Research Bioresources	
SNU-449	This study	Shanghai Cell Bank Type Culture Collection Committee	
Primers			
Name	Forward-primer		Reverse-primer
EIF2S2-qPCR	CCAGAGCCAACTGAGGACAA		ACATCACTTTCAATCTTTACACCTT
β-actin-qPCR	AGTGTGACGTGGACATCCGCAAAG		ATCCACATCTGCTGGAAGGTGGAC
PAR1-qPCR	TTTCCAGCTTTCCCACCCTC		CATGGGGCTATATCTGGGGC
SMAD4-qPCR	GCTGCAGAGCCCAGTTTAGA		CCCCAAAGCAGAAGCTACGA
ROCK2-qPCR	TCCCGATAACCACCCCTCTT		GGAAAAAGGCTTTCCAGCCG
EIF2S2-OUT	CGGAATTCCGGTGGAGCGTTAATTACATAAGAGGCACTGAT		CGGGATCCCGTGTGGCGCGAGTTACCAGGCGACGCCGCGTCGCCAGGC
EIF2S2-IN	CGGAATTCCGTCGCCTGG TAACTCGCGCC ACAC		GGACTAGTCCCGGGATCCCGTGGAGCGTT AATTACATAAGAGG
LINC01600-northern	AACGGCCTACAGTGGCTTACAAC		GGACTAGTCCGGAGCCACTCTGCCAGCCAG
LINC01600-sense	GAGCGGATGCCACCCCGTTTCCA		AAGATAAGTAACATTTTTTAATTG
LINC01600-antisense	CAATTAAAAAATGTTACTTATCTT		GAGCGGATGCCACCCCGTTTCCA

MCM3-ORF	AGTCATCCTGGGAACCTCCA	AGTCATCCTGGGAACCTCCA
CDC6-qPCR	AAGGGCGTTGGGGTCATAAG	GGCTTCATCTAAGGGCAGCA
PRRT2-qPCR	CTCCCTCCCTCCCTAGCTG	GAATAGCAGAGACAGCGGCA
CCND1-qPCR	TGAGGGACGCTTTGTCTGTC	GCCTTTGGCCTCTCGATACA
CK2-qPCR	GCCTTTGGCCTCTCGATACA	CAGCTGGGGGTAAGACCTTG
AXIN-qPCR	CAGCTGATCGATCCTGCCAT	ATATGCCCTTCCCTGTCCCT
APC-qPCR	GGAAATTCCCGGGGCAGTAA	GCCTGGTTCATGAGCTTCCT
P15-qPCR	GGGACTAGTGGAGAAGGTGC	CATCATCATGACCTGGATCGC
P21-qPCR	AGCTGCCGAAGTCAGTTCCTT	GTTCTGACATGGCGCCTCCT
BIM-qPCR	GTATTCGGTTCGCTGCGTTC	CGCAGGCTGCAATTGTCTAC
GSK3β-qPCR	GACTAAGGTCTTCCGACCCC	AAGAGTGCAGGTGTGTCTCG
MAPK1-qPCR	ACTTCAGGGGTGCCACATTC	CCTCCCGCAGGGATCTGC
CDKN2A-qPCR	ACTTCAGGGGTGCCACATTC	CGACCCTGTCCCTCAAATCC
CCNT1-qPCR	TAACTCGGCTACGGGGTGTA	CTAAGAGGCGACCCACATCC
HDAC3-qPCR	ATTGCCTCTGGCTTACCTCC	GTCTGGGATTGTGTGAACGC
LINC01600-qPCR	TGGGATGAAGACTCAACGGC	CGGGAGTTGTAAGCCACTGT
FHIT-qPCR	GAAGCCGGACAGACTGTGAA	TGCTGCCATTTCCTCCTCTG
FHIT-S1F1	CGGAATTCCGGCACTGCCACATCCCCACGGTCA	CGGGATCCCGTTTAAAAGCAGCCTGTTTCTGTC
FHIT-S1F2	CGGAATTCCGGGTCTGTGGCCTTGAAAGAGCA	CGGGATCCCGCCCAAGGTCACACAGTTGGT
FHIT-S1F3	CCGCTCGAGCGGGTGGACACAGGCCGGCAGCCATG	GGACTAGTCCTGGCTTCAGCCTGCGGCCTGA
FHIT-S1F4	CGGGATCCCGCCGGGAACAGAGGGCAAAAAGTCCT	GGACTAGTCCGGTCAGTGTTTCCCGCCCC T
FHIT-S1F5	CGGAATTCCGGACATATGCATGCTGTCTGCTTTTAA	CGGGATCCCGACCCTACTGAGATCACAGCTTGGAC
Deposited Data		
TCGA RNA sequencing data	Genomic Data Commons	https://portal.gdc.cancer.gov/
Cancer Cell Line Encyclopedia	The Broad Institute	https://portals.broadinstitute.org/ccle
TCGA clinical data	Genomic Data Commons	https://portal.gdc.cancer.gov/
MYC-ChIP-Seq	Gene Expression Omnibus	GSM1239473
DNase-Seq	ENCODE	ENCSR503BEM_rep1
DNase-Seq	ENCODE	ENCSR503BEM_rep2
Software and Algorithms		
TCGAbiolinks	R Package	https://bioconductor.org/packages/release/bioc/html/TCGAbiolinks.ht ml
Gene Set Enrichment Analysis (GSEA)	Java package	http://software.broadinstitute.org/gsea/index.jsp
R (v3.5.1)	CRAN	https://cran.r-project.org/
ggplot2	R package	https://cran.r-project.org/web/packages/ggplot2/index.html
survival	R package	https://cran.r-project.org/web/packages/survival/index.html
bedtools		https://bedtools.readthedocs.io/en/latest/
liftover	UCSC	http://genome.ucsc.edu/cgi-bin/hgLiftOver
pheatmap	R package	https://cran.r-project.org/web/packages/pheatmap/